

BOLT-GAN: Bayes-Error-Motivated Objective for Stable GAN Training

Mohammadreza Tavasoli Naeini
University of Toronto

mohammadreza.tavasolinaeini@mail.utoronto.ca

Ali Bereyhi
University of Toronto

ali.bereyhi@utoronto.ca

Morteza Noshad
Stanford University

noshad@stanford.edu

Ben Liang
University of Toronto

liang@ece.utoronto.ca

Alfred O. Hero III
University of Michigan

hero@eecs.umich.edu

Abstract

We introduce BOLT-GAN, a novel framework for stable GAN training using the Bayes optimal learning threshold (BOLT). The discriminator is trained via the BOLT loss under a standard 1-Lipschitz constraint. This guides the generator to maximize the Bayes error of the discrimination task. We show that the training objective in this case represents a class of metrics on probability measures controlled by a 1-Lipschitz discriminator minimizing an integral probability metric that is upper-bounded by Wasserstein-1 distance. Across four standard image-generation benchmarks, BOLT-GAN improves FID and precision/recall over benchmark GAN frameworks under identical architectures and training budgets. Our experimental findings further confirm the advantage of linking the GAN training objective to a min-max Bayes error criterion. Implementation software is available in our anonymous repository.

1 Introduction

The Bayes optimal learning threshold (BOLT) (Naeini et al., 2025) is a recently proposed framework for discriminative learning. In its basic form, BOLT provides a computational approach to upper-bound (and tightly approximate) the Bayes error rate (BER) by sampling an arbitrary bounded learning model. Minimizing the resulting *BOLT loss*, aligns the model with a Bayes optimal, i.e., maximum-a-posteriori (MAP), classifier.

Generative adversarial networks (GANs) learn data distribution through a two-player game between a generator and a discriminator. Despite their success, vanilla GANs trained with the cross-entropy loss and Jensen-Shannon divergence are notoriously unstable, often suffering from vanishing gradients and mode collapse. Since the discriminator’s role is inherently a binary classification task (*real* versus *fake*), it is natural to ask whether a Bayes-error-motivated discriminator objective can improve generative training dynamics. In this work, we embed the BOLT loss inside the adversarial game: we train the discriminator with the BOLT objective and train the generator to maximize the induced Bayes error rate of the discrimination task. We refer to this adversarial formulation as a *maximum Bayes error* (Max-BER) game.

Our analysis further shows that the Max-BER game induces a discrepancy between the data distribution and the generator distribution that is controlled by the discriminator. With unregularized bounded-discriminator,

this game reduces under balanced priors to minimizing the total variation (TV), a strong metric. This can yield poor gradient propagation and severe numerical instability. By restricting the discriminator class to bounded 1-Lipschitz functions, we obtain a weaker but smoother metric: an integral probability metric (IPM) that is upper-bounded by the Wasserstein-1 distance. We refer to this constrained min-max formulation as BOLT-GAN. Unlike existing GAN formulations, BOLT-GAN provides both a Bayesian interpretation of adversarial training and a pathway to improved stability.

1.1 Background and Related Work

Bayes error estimation The Bayes error rate (BER) characterizes the minimum achievable classification error for a given data-generating process (Bishop, 2006). Classical BER bounds and estimators are often expressed via distance-like quantities between class-conditional distributions (e.g., Bhattacharyya- or Mahalanobis-type measures), but they can be inaccurate in high dimensions and under model mismatch (Devroye et al., 1996). Modern nonparametric approaches estimate BER using nearest-neighbor and local neighborhood constructions (Moon et al., 2017; Noshad et al., 2019). The Bayes optimal learning threshold (BOLT) framework (Naeini et al., 2025) provides a universal upper bound on BER based on *bounded* discriminator outputs and induces a surrogate loss (the BOLT loss) whose minimization aligns a model with the Bayes-optimal, i.e. maximum-a-posteriori (MAP), classifier.

GAN A GAN trains a generator and a discriminator via a min-max game (Goodfellow et al., 2014). The original GAN training objective corresponds to optimizing the Jensen-Shannon (JS) divergence between the generative and data distributions. This basic approach is known to suffer from gradient saturation and instability, especially when the model and data supports have limited overlap (Goodfellow et al., 2014; Arjovsky et al., 2017). Alternatives replace JS with other metrics and discrepancies, e.g. f -divergence (Nowozin et al., 2016), least-squares losses (Mao et al., 2017), and auto-encoding reconstruction-loss (Berthelot et al., 2017). Among these designs, Wasserstein GAN (WGAN) shows substantial training stability (Arjovsky et al., 2017). WGAN replaces JS divergence with the Wasserstein-1 distance W_1 , yielding a smoother training signal and improved stability.

Stable GAN Training A central component in WGAN training is enforcing the 1-Lipschitz constraint on the discriminator function. This is commonly addressed via gradient penalty (Gulrajani et al., 2017) or spectral normalization (Miyato et al., 2018). Other stabilization approaches include training heuristics such as progressive growing (Karras et al., 2018). Bayesian GAN formulations place priors over network parameters and sample from posterior distributions to quantify uncertainty (Saatchi & Wilson, 2017; Ye & Zhu, 2018). Several studies analyze generalization and equilibrium behavior via statistical distances for learning dynamics (Arora et al., 2017; Zhang et al., 2021). Our work complements these lines of work by directly training the discriminator for Bayes optimal discrimination via the BOLT loss.

1.2 Main Contributions

The key contributions of this work are as follows. (i) *Bayes-optimal GAN training via Max-BER*: we deploy the BOLT framework to formulate Bayes-optimal GAN training, where the generator is trained to maximize the Bayes error rate of the discrimination task. We first show the Bayes optimality of BOLT (Theorem 2) and characterize the bias and variance of the BOLT plug-in estimation of the BER (Theorem 3). We then conclude that under the Max-BER game, the generator and data distributions match in total variation (Theorem 4). (ii) *BOLT-GAN framework*: We further show that, when the discriminator is restricted to the class of Lipschitz models, the BOLT-trained GAN minimizes the distance between the generator and data distributions with respect to an alternative IPM that is bounded by the Wasserstein-1 distance (Theorem 5). The resulting BOLT-GAN trains the generator toward the true data distribution using a weaker notion of distance, leading to more efficient gradient backpropagation and hence better stability. (iii) *Empirical validation*: We validated BOLT-GAN through experiments with the CIFAR-10, CelebA-64, LSUN Bedroom-64, and LSUN Church-64 datasets. We report FID, precision, and recall, and compare against WGAN and HINGE-GAN baselines (Miyato et al., 2018).

Notation On a measurable space $(\mathcal{X}, \mathcal{F})$, probability measures are shown uppercase, e.g., P , and their corresponding densities are denoted lowercase, e.g., p . Expectation with respect to probability measure P is shown by $\mathbb{E}_{X \sim P}[\cdot]$. The set $\{1, \dots, n\}$ is abbreviated as $[n]$.

2 Preliminaries

We consider binary classification with classes $C \in \{1, 2\}$ and data space $\mathcal{X} \subseteq \mathbb{R}^d$. Let $q_i := \Pr(C = i)$ denote the class priors ($q_2 = 1 - q_1$), and let P_i denote the class-conditional distribution of X given $C = i$. When needed, assume P_i admits a density p_i with respect to a common dominating measure μ on \mathcal{X} .

The Bayes error rate (BER), denoted by $\varepsilon_{\text{Bayes}}$, is the minimum error probability achievable by any measurable classifier $f : \mathcal{X} \rightarrow \{C_1, C_2\}$, which is achieved by the maximum a posteriori (MAP) rule (Bishop, 2006). In terms of densities, the BER is

$$\varepsilon_{\text{Bayes}} = 1 - \int_{\mathcal{X}} \max_{i \in \{1, 2\}} \{q_i p_i(x)\} d\mu(x), \quad (1)$$

and the MAP classifier assigns sample x to

$$\hat{C}(x) \in \arg \max_{i \in \{1, 2\}} q_i p_i(x). \quad (2)$$

2.1 BOLT Framework

With unknown data distribution, the BER can be approximated (Devroye et al., 1996; Fukunaga, 2013; Noshad et al., 2019). Naeini et al. (2025) have developed an empirical estimate of universal upper bound on BER that can be computed by sampling an arbitrary measurable and bounded function (e.g., a neural network). The resulting surrogate objective given by this upper bound is called the BOLT risk.

The following theorem presents the universal bound for binary classification.

Theorem 1 (Binary Bayes error (Naeini et al., 2025)). *Let $h : \mathcal{X} \rightarrow [0, 1]$ be a measurable function. Then, the BER is bounded as¹*

$$\varepsilon_{\text{Bayes}} \leq q_1 + q_2 \mathbb{E}_{X \sim P_2}[h(X)] - q_1 \mathbb{E}_{X \sim P_1}[h(X)]. \quad (3)$$

Naeini et al. (2025) show that the bound (3) is tight when optimized over h . This enables a computational means to estimate $\varepsilon_{\text{Bayes}}$ by sampling the output of a bounded computational model h with parameters θ . This transforms the upper bound in Theorem 1 into a training objective referred to as the Bayes optimal learning threshold (BOLT). While Naeini et al. (2025) establish the BOLT loss for a general multi-class problem, we focus on the binary case relevant to the discrimination component of GANs.

BOLT loss Considering a labeled dataset $\mathcal{D} = \{(x_i, C_i) : i \in [n]\}$, where $C_i \in \{1, 2\}$. BOLT trains the model $h_\theta : \mathcal{X} \rightarrow [0, 1]$ by minimizing an empirical surrogate of the bound in Theorem 1. This can be seen as an empirical risk minimization *problem*, where each $(x, C) \in \mathcal{D}$ is a (feature,label) sample and the BOLT loss is given by

$$\ell_{\text{BOLT}}(h_\theta(x), C) = (-1)^C h_\theta(x). \quad (4)$$

The bound in Theorem 1 can be directly written in terms of BOLT risk as

$$\varepsilon_{\text{Bayes}} \leq q_1 + \mathbb{E}[\ell_{\text{BOLT}}(h_\theta(X), C)], \quad (5)$$

where the expectation is over (X, C) generated as $\Pr(C = i) = q_i$ and $X \mid \{C = i\} \sim P_i$, for $i \in \{1, 2\}$.

2.2 Generative Adversarial Networks

A GAN consists of two functions: a generator $g : \mathcal{Z} \rightarrow \mathcal{X}$ that maps a latent variable $Z \sim P_Z$ to a sample in data space \mathcal{X} , and a discriminator $h : \mathcal{X} \rightarrow [0, 1]$ that distinguishes generated samples $g(Z)$ from true data samples $X \sim P_{\text{data}}$. We denote the induced distribution of $g(Z)$ by P_g .

¹The result in Naeini et al. (2025) is given for $\tilde{h} : \mathcal{X} \rightarrow [-1, 0]$. We represent the result after the reparameterization $h = 1 + \tilde{h}$.

Vanilla GAN The vanilla training approach, proposed in the initial study by Goodfellow et al. (2014), treats the discrimination as a classic binary classification problem. In this sense, it sets $h(x) = P(C = \text{real}|x)$ and uses the cross-entropy loss to train it. This approach implicitly implements the maximum likelihood training of the generator (Arjovsky et al., 2017). The risk function, i.e., the expected loss used for training, in this case is given by

$$R_{\text{ML}}(g, h) = \mathbb{E} [\text{CE}(Y, C)], \quad (6)$$

where CE denotes the cross-entropy loss function, Y is the output of the discriminator, i.e., $Y = h(X)$, for an input $X \in \mathcal{X}$ to the discriminator, and $C \in \{1, 2\}$ is the label of X with $C = 1$ and $C = 2$ denoting **real** and **fake** inputs respectively. Where C is sampled from a prior $\pi = \Pr\{C = 1\}$ for some $\pi \in (0, 1)$,² and X is sampled conditionally from $P_1 = P_{\text{data}}$ and $P_2 = P_g$.

Noting that $P_2 = P_g$ is the distribution of $g(Z)$ computed from the latent sample $Z \sim P_Z$, we can use the definition of cross-entropy to expand the risk in (6) as

$$\begin{aligned} R_{\text{ML}}(g, h) &= -\pi \mathbb{E}_{X \sim P_{\text{data}}} [\log h(X)] \\ &\quad - (1 - \pi) \mathbb{E}_{Z \sim P_Z} [\log(1 - h(g(Z)))] . \end{aligned} \quad (7)$$

Defining $\mathcal{L}_{\text{ML}}(g, h) = -R_{\text{ML}}(g, h)$, the generator learns to sample P_{data} by the following min-max game

$$\min_g \max_h \mathcal{L}_{\text{ML}}(g, h), \quad (8)$$

which is equivalent to fooling the best discriminator. It is shown that the solution to this min-max game, when solved for any measurable generator g and discriminator h , guarantees the convergence of P_g to P_{data} as measured by the convergence of the Jensen–Shannon (JS) divergence to zero (Goodfellow et al., 2014, Theorem 1).

Wasserstein GAN Arjovsky et al. (2017) propose to train the generator–discriminator pair by minimizing the Wasserstein-1 distance (Earth Mover distance) between P_{data} and P_g . Using the Kantorovich–Rubinstein duality, this distance can be written as a supremum over 1-Lipschitz functions; accordingly, the WGAN “discriminator” is a real-valued *critic* (rather than a probabilistic classifier) and is constrained to be 1-Lipschitz in theory. In practice, this constraint is typically enforced via weight clipping, gradient penalty, or spectral normalization (see the supplementary material for additional discussion). This yields the min–max objective (Arjovsky et al., 2017, Theorem 3)

$$\mathcal{L}_{\text{EM}}(g, h) = \mathbb{E}_{X \sim P_{\text{data}}} [h(X)] - \mathbb{E}_{Z \sim P_Z} [h(g(Z))]. \quad (9)$$

Learning proceeds by solving the same min-max game as in (8) with $\mathcal{L}_{\text{EM}}(g, h)$ as the objective. While WGAN still guarantees convergence of P_g to P_{data} , the notion of convergence is in Wasserstein distance (a weaker topology than that induced by common information divergences), which often leads to improved training stability compared with vanilla GAN (Arjovsky et al., 2017).

3 GAN with Maximum BER

Discriminator training in GANs is inherently a *binary classification* problem (**real** versus **fake**), which motivates using BOLT. However, deploying BOLT inside the adversarial game requires understanding how the Bayes-optimal discriminator is estimated from a BOLT-trained model. In the sequel, we characterize this connection by showing that a population BOLT minimizer recovers the Bayes optimal discriminator by thresholding. We further derive a finite-sample guarantee for a plug-in BER estimator computed by empirical BOLT risk. These results enable us to formulate the GAN training via a min-max problem, in which the generator is trained adversarially to increase the discriminator-induced BER. We characterize the metric under which P_g converges to P_{data} .

²Typically, $\pi = 0.5$ is considered.

3.1 Bayes Optimal Discriminator via BOLT

Naeini et al. (2025) conjectured that a model trained via *empirical* BOLT risk can estimate the Bayes optimal classifier, and proposed a heuristic plug-in rule based on thresholding the learned score h . In the sequel, we formalize this connection. Theorem 2 shows that any population minimizer of the BOLT risk is Bayes-aligned and that thresholding at $1/2$ recovers the MAP decision rule.

Theorem 2 (MAP vs. BOLT optimum). *Consider the binary classification setup in Section 2 and let P_X denote the marginal distribution of X . Let*

$$h^* \in \arg \min_{h: \mathcal{X} \rightarrow [0,1]} \mathbb{E}[\ell_{\text{BOLT}}(h(X), C)]. \quad (10)$$

and

$$\eta(x) := \Pr(C = 1 \mid X = x) \quad (11)$$

be the likelihood of x . Then, for P_X -a.e. x , we have

$$h^*(x) = \begin{cases} 1, & \eta(x) > \frac{1}{2}, \\ 0, & \eta(x) < \frac{1}{2}, \\ z, & \eta(x) = \frac{1}{2}. \end{cases} \quad (12)$$

for some $z \in [0, 1]$. Consequently, the plug-in classifier

$$\hat{C}(x) = \begin{cases} 1, & h^*(x) \geq \frac{1}{2}, \\ 2, & h^*(x) < \frac{1}{2}, \end{cases} \quad (13)$$

coincides P_X -a.e. with the MAP classifier

$$C_{\text{MAP}}(x) \in \arg \max_{k \in \{1,2\}} \Pr\{C = k \mid X = x\}. \quad (14)$$

Proof. See Appendix B. □

Theorem 2 further enables us to express the MAP classifier in terms of the likelihood ratio and rewrite the Bayes error as a hinge expectation.

Corollary 1 (Optimal BOLT function and hinge form of $\varepsilon_{\text{Bayes}}$). *Assume $q_1, q_2 > 0$ and that P_1, P_2 admit densities p_1, p_2 w.r.t. a common dominating measure. Define the likelihood ratio $U(x) := p_1(x)/p_2(x)$ on $\{p_2(x) > 0\}$ and the prior threshold $\tau := q_2/q_1$. Then a pointwise optimizer of the BOLT functional over $h : \mathcal{X} \rightarrow [0, 1]$ is*

$$h^*(x) = \begin{cases} 0, & U(x) < \tau, \\ 1, & U(x) \geq \tau, \end{cases} \quad (15)$$

and, defining the hinge map $t_0(u) := [q_2 - q_1 u]_+$, one has

$$\mathcal{L}_{\text{BOLT}}(h^*) = \varepsilon_{\text{Bayes}} = q_2 - \mathbb{E}_{X \sim P_2}[t_0(U(X))]. \quad (16)$$

Proof. For x with $p_2(x) > 0$, Bayes' rule gives

$$\eta(x) := \Pr(C = 1 \mid X = x) = \frac{q_1 U(x)}{q_1 U(x) + q_2}. \quad (17)$$

Hence, $\eta(x) \geq \frac{1}{2}$ iff $U(x) \geq \tau$ with $\tau := q_2/q_1$. Substituting this relation into Theorem 2 yields (15). The hinge representation (16) follows by rewriting the tight BOLT bound at h^* in terms of U . □

Corollary 1 shows that $\varepsilon_{\text{Bayes}}$ can be written as an expectation of a hinge of U . In practice, a discriminator trained via *empirical* BOLT risk can be used to form a finite-sample likelihood-ratio estimate \widehat{U} (see Appendix B). Plugging \widehat{U} into Corollary 1, we can estimate the MAP classifier and BER. The following result characterizes the bias and variance of the BER estimator.

Theorem 3 (BER estimator). *Let $\widehat{U} : \mathcal{X} \rightarrow \mathbb{R}$ be an estimator of the likelihood ratio U , and let $\widehat{q}_1, \widehat{q}_2 \in (0, 1)$ be empirical class priors computed on M samples. Define $\widehat{\varepsilon}_{\text{BOLT}}$ as the plug-in estimator obtained from the hinge representation in Corollary 1 by sample averaging with M samples. Assume $\mathbb{E}_{X \sim P_2} [|\widehat{U}(X) - U(X)|] \leq \varepsilon_0$. Then, we have*

$$|\mathbb{E}[\widehat{\varepsilon}_{\text{BOLT}}] - \varepsilon_{\text{Bayes}}| \leq q_1 \varepsilon_0 + O(M^{-1/2}), \quad (18)$$

and

$$\text{Var}(\widehat{\varepsilon}_{\text{BOLT}}) = O(M^{-1}). \quad (19)$$

Proof. See Appendix B. □

3.2 Generation with Maximum BER

The results of Section 3.1 allow us to interpret a BOLT-trained discriminator as an estimator of the Bayes-optimal classifier for the real-fake classification task, and to view its objective as a tight surrogate for the discrimination BER. We therefore construct an adversarial objective where, for a fixed generator g , the discriminator h is trained via the (population) BOLT risk under prior π , and the generator is trained to *maximize* the induced BER (equivalently, minimize the discriminator best achievable performance). Intuitively, this pushes P_g toward P_{data} by making real and fake samples maximally confusable. We characterize this behavior by showing that the resulting maximum BER problem minimizes the TV between P_{data} and P_g .

Maximum BER objective Consider a GAN with generator g and a bounded discriminator $h : \mathcal{X} \rightarrow [0, 1]$. Let P_g denote the distribution of $g(Z)$ for $Z \sim P_Z$, and define $\pi = \Pr\{C = 1\}$, i.e. probability of sampling a real data-point. We train h by the empirical BOLT risk, and train g adversarially to maximize the induced discrimination BER. Following the BOLT formulation, the discrimination BER is estimated (up to a constant) via

$$\max_h \mathcal{L}_{\text{BG}}^{(\pi)}(g, h), \quad (20)$$

where $\mathcal{L}_{\text{BG}}^{(\pi)}(g, h)$ is defined as³

$$\begin{aligned} \mathcal{L}_{\text{BG}}^{(\pi)}(g, h) &:= \pi \mathbb{E}_{X \sim P_{\text{data}}} [h(X)] \\ &\quad - (1 - \pi) \mathbb{E}_{Z \sim P_Z} [h(g(Z))]. \end{aligned} \quad (21)$$

By Theorem 2, thresholding the BOLT-optimal discriminator yields the Bayes optimal discrimination rule. Accordingly, the generator can adversarially fool the Bayes optimal discrimination by solving the Max-BER problem that is given by

$$\min_g \max_h \mathcal{L}_{\text{BG}}^{(\pi)}(g, h). \quad (22)$$

Generator distribution Intuitively, the Max-BER problem leads to learning data distribution. We next show this and characterize the metric, under which the generator distribution P_g converges to P_{data} . To this end, let us first define total variation (TV).

³Note that $\mathcal{L}_{\text{BG}}^{(\pi)}(g, h)$ is the negative of the (population) BOLT risk, up to the additive constant π .

Definition 1 (Total variation norm). *The total variation between two distributions P and Q defined on a measurable space (X, \mathcal{B}) is defined as*

$$\text{TV}(P, Q) = \sup_{A \in \mathcal{B}} |P(A) - Q(A)|, \quad (23)$$

where \mathcal{B} is the σ -algebra on \mathcal{X} .

In the sequel, we use the standard variational representation of TV given in the following lemma.

Lemma 1 (Dudley (2002a)). *The total variation between P and Q is equivalently given by*

$$\text{TV}(P, Q) = \sup_{f: \mathcal{X} \rightarrow [0, 1]} \int f d(P - Q), \quad (24)$$

where the difference $P - Q$ is a signed measure on \mathcal{B} .

The following theorem characterizes the connection between the BOLT-GAN learning objective $\mathcal{L}_{\text{BG}}^{(\pi)}$ and the TV between the generator and the data distributions.

Theorem 4 (BOLT vs TV). *Fix the prior $\pi \in (0, 1)$. For generator g , let P_g denote the distribution of $g(Z)$, when $Z \sim P_Z$. Define $\mathcal{D}^{(\pi)}$ as*

$$\mathcal{D}^{(\pi)}(g) \triangleq \sup_h \mathcal{L}_{\text{BG}}^{(\pi)}(g, h), \quad (25)$$

with the maximum taken over all bounded discriminators, i.e., all $h: \mathcal{X} \mapsto [0, 1]$. Then, $\mathcal{D}^{(\pi)}$ satisfies

$$\mathcal{D}^{(\pi)}(g) + \mathcal{D}^{(1-\pi)}(g) \geq \text{TV}(P_{\text{data}}, P_g). \quad (26)$$

with equality holding when $\pi = 0.5$.

Proof. From the definition (21), we have

$$\begin{aligned} \mathcal{L}_{\text{BG}}^{(\pi)}(g, h) + \mathcal{L}_{\text{BG}}^{(1-\pi)}(g, h) &= \mathbb{E}_{X \sim P_{\text{data}}}[h(X)] \\ &\quad - \mathbb{E}_{Z \sim P_Z}[h(g(Z))]. \end{aligned} \quad (27)$$

Noting that $g(Z)$ has distribution P_g , we can write

$$\begin{aligned} \mathcal{L}_{\text{BG}}^{(\pi)}(g, h) + \mathcal{L}_{\text{BG}}^{(1-\pi)}(g, h) &= \mathbb{E}_{X \sim P_{\text{data}}}[h(X)] \\ &\quad - \mathbb{E}_{X \sim P_g}[h(X)]. \end{aligned} \quad (28)$$

Then

$$\Sigma(g) \triangleq \sup_{h: \mathcal{X} \mapsto [0, 1]} \left[\mathcal{L}_{\text{BG}}^{(\pi)}(g, h) + \mathcal{L}_{\text{BG}}^{(1-\pi)}(g, h) \right] \quad (29)$$

$$= \sup_{h: \mathcal{X} \mapsto [0, 1]} \left[\int h(X) d(P_{\text{data}} - P_g) \right] \quad (30)$$

$$\stackrel{(a)}{=} \text{TV}(P_{\text{data}}, P_g), \quad (31)$$

where (a) follows from Lemma 1. We next use the fact that

$$\Sigma(g) \leq \sup_h \left[\mathcal{L}_{\text{BG}}^{(\pi)}(g, h) \right] + \sup_h \left[\mathcal{L}_{\text{BG}}^{(1-\pi)}(g, h) \right], \quad (32)$$

and the definition of $\mathcal{D}^{(\pi)}$ to conclude that

$$\text{TV}(P_{\text{data}}, P_g) = \Sigma(g) \quad (33)$$

$$\leq \mathcal{D}^{(\pi)}(g) + \mathcal{D}^{(1-\pi)}(g). \quad (34)$$

This proves the inequality. We next note that at $\pi = 0.5$

$$\begin{aligned} \text{TV}(P_{\text{data}}, P_g) &= \Sigma(g) \\ &= \sup_h \left[\mathcal{L}_{\text{BG}}^{(0.5)}(g, h) + \mathcal{L}_{\text{BG}}^{(0.5)}(h, g) \right] \\ &= 2\mathcal{D}^{(0.5)}(g). \end{aligned} \tag{35}$$

This concludes the proof. \square

Theorem 4 indicates that the solution to the Max-BER problem leads to P_g converging P_{data} in TV. In particular, under the balanced prior $\pi = 0.5$, we obtain the exact identity $\text{TV}(P_{\text{data}}, P_g) = 2\mathcal{D}^{(0.5)}(g)$, so the Max-BER problem is equivalent to minimizing TV. For general $\pi \in (0, 1)$, Theorem 4 relates TV to the pair of games specified by $\mathcal{D}^{(\pi)}(g)$ and $\mathcal{D}^{(1-\pi)}(g)$, and hence the convergence in TV is guaranteed when the worst-case objective converges to zero.

Corollary 2 (Half-TV guarantee). *Let $\mathcal{D}^{(\pi)}$ be defined as in Theorem 4. Assume for a given generator g , we have*

$$\max \left\{ \mathcal{D}^{(\pi)}(g), \mathcal{D}^{(1-\pi)}(g) \right\} \leq \varepsilon. \tag{36}$$

Then, the TV between the generator and data distributions is bounded as

$$\text{TV}(P_{\text{data}}, P_g) \leq 2\varepsilon. \tag{37}$$

Proof. Using Theorem 4, we have

$$\begin{aligned} 2 \max \left\{ \mathcal{D}^{(\pi)}(g), \mathcal{D}^{(1-\pi)}(g) \right\} &\geq \mathcal{D}^{(\pi)}(g) + \mathcal{D}^{(1-\pi)}(g) \\ &\geq \text{TV}(P_{\text{data}}, P_g). \end{aligned} \tag{38}$$

This concludes the proof. \square

4 BOLT-GAN Framework

With an unregularized bounded-discriminator, i.e., the Max-BER setting, the optimal discriminator may be highly non-smooth, and the training of a parameterized model can be unstable. Theorem 4 shows that under balanced priors this problem is directly linked to TV, a strong discrepancy that can yield poorly behaved gradients in adversarial optimization. For stable training, we propose BOLT-GAN, which solves the Max-BER problem while restricting the discriminator to be 1-Lipschitz.

More precisely, BOLT-GAN solves the following *constrained* Max-BER problem

$$\min_g \max_{h \in \mathcal{H}_{\text{Lip}}} \mathcal{L}_{\text{BG}}^{(\pi)}(g, h), \tag{39}$$

where \mathcal{H}_{Lip} denotes the class of bounded 1-Lipschitz discriminators, i.e.,

$$\begin{aligned} \mathcal{H}_{\text{Lip}} = \{h : \mathcal{X} \mapsto [0, 1] : &|h(x) - h(y)| \leq \|x - y\| \\ &\forall x, y \in \mathcal{X}\}. \end{aligned} \tag{40}$$

We next characterize the convergence of BOLT-GAN.

4.1 BOLT-GAN Generator Distribution

Theorem 5 shows that the constrained Max-BER problem solved by BOLT-GAN minimizes an induced IPM that is upper-bounded by the Wasserstein-1 distance between P_g and P_{data} . Before stating the main result, let us define the Wasserstein-1 distance.

Definition 2 (Wasserstein-1 distance). *Let $(\mathcal{X}, \|\cdot\|)$ be a metric space and let P, Q be probability measures on \mathcal{X} with finite first moment. The Wasserstein-1 distance is*

$$W_1(P, Q) \triangleq \inf_{\gamma \in \Pi(P, Q)} \mathbb{E}_{(X, Y) \sim \gamma} [\|X - Y\|], \quad (41)$$

where $\Pi(P, Q)$ is the set of couplings of P and Q .

Computing the Wasserstein-1 distance between two general probability measures is intractable in closed form. The Kantorovich-Rubinstein duality result Villani (2009) gives an alternative formulation which enables estimating this distance by sampling.

Lemma 2 (Kantorovich-Rubinstein duality Villani (2009)). *Let P, Q be probability measures on $(\mathcal{X}, \|\cdot\|)$ with finite first moment. Then*

$$W_1(P, Q) = \sup_{f: \text{Lip}(f) \leq 1} \{\mathbb{E}_{X \sim P}[f(X)] - \mathbb{E}_{X \sim Q}[f(X)]\}.$$

We next present the Theorem 5, which characterizes the converging behavior of the generator when trained by BOLT-GAN.

Theorem 5 (BOLT-GAN Convergence). *Fix $0 < \pi \leq 0.5$, for the generator g , define*

$$\mathcal{D}_{\text{Lip}}^{(\pi)}(g) \triangleq \max_{h \in \mathcal{H}_{\text{Lip}}} \mathcal{L}_{\text{BG}}^{(\pi)}(g, h), \quad (42)$$

with $\mathcal{L}_{\text{BG}}^{(\pi)}(g, h)$ defined in (21). Then, for any prior $0 < \pi \leq 0.5$, we have

$$\mathcal{D}_{\text{Lip}}^{(\pi)}(g) \leq W_1(P_{\text{data}}, P_g). \quad (43)$$

where W_1 denotes the Wasserstein-1 distance.

Proof. Starting with (28) in the proof of Theorem 4, we can write

$$\Sigma_{\text{Lip}}(g) \triangleq \sup_{h \in \mathcal{H}_{\text{Lip}}} [\mathcal{L}_{\text{BG}}^{(\pi)}(g, h) + \mathcal{L}_{\text{BG}}^{(1-\pi)}(g, h)] \quad (44)$$

$$= \sup_{h \in \mathcal{H}_{\text{Lip}}} \left\{ \mathbb{E}_{X \sim P_{\text{data}}}[h(X)] - \mathbb{E}_{X \sim P_g}[h(X)] \right\}. \quad (45)$$

In the Appendix C, we show that for $0 < \pi \leq 0.5$,

$$\mathcal{D}_{\text{Lip}}^{(\pi)}(g) \leq \Sigma_{\text{Lip}}(g). \quad (46)$$

We can hence write

$$\mathcal{D}_{\text{Lip}}^{(\pi)}(g) \leq \sup_{h \in \mathcal{H}_{\text{Lip}}} \left\{ \mathbb{E}_{X \sim P_{\text{data}}}[h(X)] - \mathbb{E}_{X \sim P_g}[h(X)] \right\}.$$

Let $\mathcal{H}_{\text{Lip}}^+$ denotes the set of 1-Lipschitz functions, i.e.,

$$\mathcal{H}_{\text{Lip}}^+ = \{h : |h(x) - h(y)| \leq \|x - y\| \forall x, y \in \mathcal{X}\}.$$

Noting that $\mathcal{H}_{\text{Lip}} \subset \mathcal{H}_{\text{Lip}}^+$, we can use the Kantorovich-Rubinstein duality to write

$$\begin{aligned} & W_1(P_{\text{data}}, P_g) \\ & \geq \sup_{h \in \mathcal{H}_{\text{Lip}}} \left\{ \mathbb{E}_{X \sim P_{\text{data}}}[h(X)] - \mathbb{E}_{X \sim P_g}[h(X)] \right\}, \end{aligned} \quad (47)$$

$$\geq \mathcal{D}_{\text{Lip}}^{(\pi)}(g), \quad (48)$$

which concludes the proof. \square

We note that $\mathcal{D}_{\text{Lip}}^{(\pi)}(g)$ is an IPM between P_g and P_{data} , and it is minimized by BOLT-GAN as indicated in (39). Theorem 5 implies that convergence in the Wasserstein-1 distance suffices to guarantee convergence in the BOLT-GAN IPM, while the converse does not necessarily hold. Our numerical experiments further show that this weaker distance metric leads to more stable training.

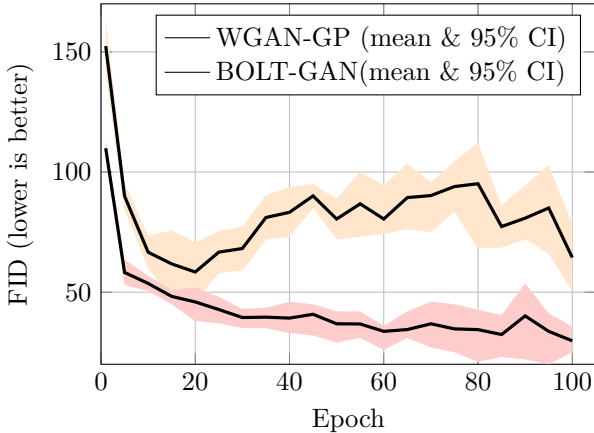


Figure 1: CIFAR-10 FID vs. epochs (mean and 95% confidence interval over 3 seeds), showing consistently improved convergence of BOLT-GAN relative to WGAN-GP.

4.2 Computational Lipschitz Enforcement

In practice, we parameterize the discriminator as $h_\theta(X) = \sigma(f_\theta(x))$ for some score function $f_\theta(x)$, where σ denotes the sigmoid function. The 1-Lipschitz constraint is computationally enforced on the score f_θ using a gradient penalty (GP) (Gulrajani et al., 2017): for $\hat{X} = \varepsilon X + (1 - \varepsilon)g(Z)$ with $\varepsilon \sim \text{Unif}(0, 1)$, we add

$$\lambda_{\text{GP}} \mathbb{E} \left(\|\nabla_{\hat{X}} f_\theta(\hat{X})\|_2 - 1 \right)^2 \quad (49)$$

to the discriminator loss for some regularizer λ_{GP} . Since the sigmoid function σ is Lipschitz, this enforcement implies that h is also Lipschitz.⁴

5 Experiments and Results

To evaluate the proposed BOLT-GAN, we conduct unconditional image-generation experiments on four standard benchmarks: CIFAR-10, CelebA-64, LSUN Bedroom-64, and LSUN Church-64. We compare against (i) WGAN, since it uses the same 1-Lipschitz enforcement mechanism as our implementation, and (ii) a HINGE-GAN, a widely used stability-focused baseline. Unless otherwise stated, BOLT-GAN and WGAN use the *same* generator and discriminator architectures and optimizer settings, i.e., the only difference is the training objective. In the experiments, we report the Fréchet inception distance (FID), as well as Improved Precision and Recall (Kynkänniemi et al., 2019) to quantify sample fidelity and mode coverage.

5.1 Experimental Setup

We use a residual DCGAN backbone (Gulrajani et al., 2017): the generator maps a 128-D Gaussian latent vector to images via residual upsampling blocks, and the discriminator mirrors this with residual downsampling, global-sum pooling, and a linear head. The generator uses BatchNorm and ReLU, and the discriminator uses LeakyReLU. BOLT-GAN and WGAN enforce 1-Lipschitzness via gradient penalty, while HINGE-GAN uses the hinge discriminator loss with spectral normalization (Miyato et al., 2018). We train with batch size 64 using Adam optimizer with parameters $\alpha = 2 \times 10^{-4}$, $\beta_1 = 0.5$, and $\beta_2 = 0.999$, for 20 epochs unless noted. We report FID computed with `pytorch-fid` (Seitzer, 2020) on 10,000 generated samples (FID@10k) and Improved Precision and Recall with ($n = 2000$, $k = 3$) using 2000 generated and 2000 real samples. Unless stated otherwise, results are averaged over N seeds, curves show mean \pm std. Tables report either the value at a fixed epoch budget or the best value within the stated budget, as specified in the captions.

⁴Indeed, h is Lipschitz with $\text{Lip}(h) \leq \text{Lip}(\sigma) \text{Lip}(f_\theta)$.

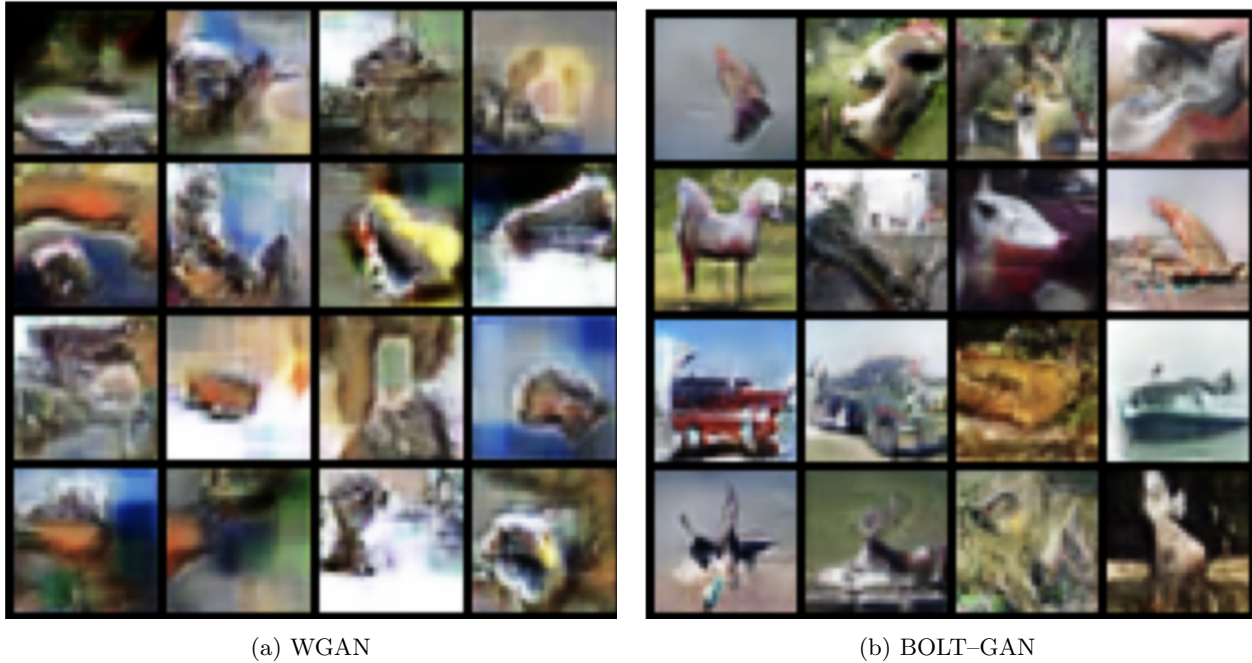


Figure 2: CIFAR-10 samples at 100 epochs.

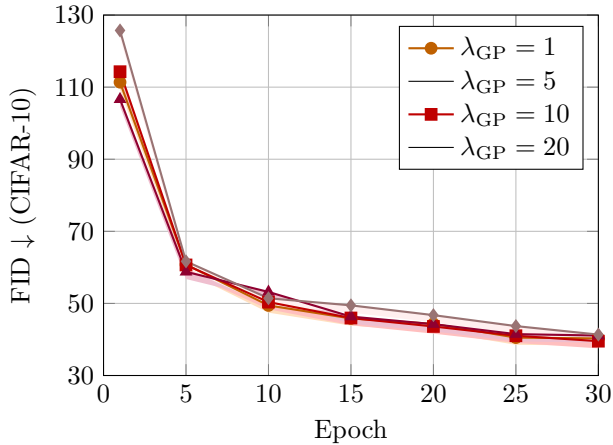


Figure 3: CIFAR-10 FID vs. epochs for different λ_{GP} (mean \pm std, 3 seeds).

5.2 Quantitative Results

Figure 1 shows the CIFAR-10 FID trajectory over training, where BOLT-GAN consistently achieves lower FID than WGAN-GP across epochs. Table 1 reports FID after 20 epochs. BOLT-GAN improves substantially over WGAN across all datasets and is competitive with (and in several cases slightly better than) HINGE-GAN under the same compute budget. To quantify mode coverage, Table 2 reports Precision and Recall (higher is better). Across datasets where we computed the metric, BOLT-GAN improves both precision and recall relative to WGAN, indicating better quality *and* coverage. Figure 2 shows CIFAR-10 samples after 100 epochs, where BOLT-GAN yields sharper images with fewer artifacts compared to WGAN.

Table 3 compares Lipschitz discriminator ($\lambda_{GP} = 10$) with an unconstrained one ($\lambda_{GP} = 0$). The results show that removing Lipschitz enforcement, i.e., setting $\lambda_{GP} = 0$, leads to severe numerical instability, while training via a Lipschitz-constrained discriminator remains stable.

Table 1: FID (\downarrow) after 20 epochs (mean \pm std over N seeds).

Dataset	HINGE-GAN	BOLT-GAN	WGAN
CIFAR-10	46.9 ± 0.8	44.2 ± 0.6	60.0 ± 1.0
LSUN Church-64	19.7 ± 0.5	14.8 ± 0.4	43.5 ± 0.9
LSUN Bedroom-64	28.8 ± 0.6	28.4 ± 0.5	102.5 ± 2.0
CelebA-64	19.6 ± 0.5	9.2 ± 0.3	10.3 ± 0.4

Table 2: Improved Precision/Recall (\uparrow) with $n = 2000$, $k = 3$ (higher is better). Best values per dataset/epoch are bolded.

Dataset	Epochs	Method	Precision	Recall
CIFAR-10	20	BOLT-GAN	0.763	0.352
	20	WGAN	0.714	0.183
	100	BOLT-GAN	0.812	0.469
	100	WGAN	0.764	0.102
LSUN Church-64	20	BOLT-GAN	0.750	0.411
	20	WGAN	0.681	0.176
	100	BOLT-GAN	0.792	0.502
	100	WGAN	0.731	0.098
LSUN Bedroom-64	20	BOLT-GAN	0.598	0.450
	20	WGAN	0.388	0.098
CelebA-64	20	BOLT-GAN	0.840	0.548
	20	WGAN	0.672	0.104

5.3 Ablation Studies

Label smoothing can be accomplished in BOLT-GAN by changing the prior π . Table 4 shows the FID at 20 and 100 epochs for various choices of prior π . As the results show, a modest prior imbalance can slightly improve FID on CIFAR-10.

We next test the robustness to gradient-penalty strength, we sweep $\lambda_{\text{GP}} \in \{1, 5, 10, 20\}$ for 20 epochs and report FID averaged over N seeds; see Table 5. The results show that performance stays within roughly ± 1 FID across the range. Figure 3 further reports FID trajectories across several GP strengths, showing only mild sensitivity over $\lambda_{\text{GP}} \in \{1, 5, 10, 20\}$ and motivating our default choice $\lambda_{\text{GP}} = 10$.

6 Conclusion

We proposed BOLT-GAN, a Bayes-error-motivated objective for stable GAN training that trains a bounded 1-Lipschitz discriminator with the BOLT loss. The discriminator in this case estimates a Bayes optimal binary classifier for the real-fake classification task, and the generator learns the data distribution adversarially by maximizing the discrimination BER. We showed that the Max-BER problem solved by BOLT-GAN minimized an IPM between the generator and data distributions that is upper-bounded by the Wasserstein-1 distance. In absence of Lipschitz constraint at the discriminator, the Max-BER problem minimizes the TV between the two distributions, leading to empirical instability. Experiments demonstrate that BOLT-GAN improves FID and Improved Precision/Recall over the state-of-the-art frameworks, such as WGAN and HINGE-GAN, under identical architectures and training budgets. Understanding how alternative con-

Table 3: FID (\downarrow) after 20 epochs for Max-BER (unregularized; $\lambda_{\text{GP}} = 0$) compared with the proposed BOLT-GAN (Lipschitz; $\lambda_{\text{GP}} = 10$).

Dataset	Max-BER	BOLT-GAN
CIFAR-10	352 ± 48	44.2 ± 1.2
CelebA-64	276 ± 35	9.2 ± 0.4
LSUN Church-64	468 ± 56	31.6 ± 0.7

Table 4: CIFAR-10 FID for different priors π (mean \pm std).

Prior π	FID @ 20 epochs	FID @ 100 epochs
0.50	44.2 ± 0.6	36.6 ± 0.8
0.45	45.3 ± 0.7	36.2 ± 0.7
0.40	48.5 ± 1.0	41.0 ± 1.1
0.35	51.4 ± 1.3	44.8 ± 1.4

Table 5: FID (\downarrow) of WGAN and BOLT-GAN on CIFAR-10 across different values of λ_{GP} .

λ_{GP}	1	5	10	20
WGAN	60.8	59.6	60.0	61.1
BOLT-GAN	44.3	43.6	44.2	46.7

straints at the discriminator impact the convergence behavior of the Max-BER approach for training is an interesting direction for future research.

References

Anil, C., Lucas, J., and Grosse, R. Sorting out lipschitz function approximation. In *International Conference on Machine Learning (ICML)*, pp. 291–301. PMLR, 2019.

Arjovsky, M., Chintala, S., and Bottou, L. Wasserstein Generative Adversarial Networks. In *International Conference on Machine Learning (ICML)*, pp. 214–223. PMLR, 2017.

Arora, S., Ge, R., Liang, Y., Ma, T., and Zhang, Y. Generalization and equilibrium in generative adversarial nets (gans). In *International Conference on Machine Learning (ICML)*, pp. 224–232. PMLR, 2017.

Berthelot, D., Schumm, T., and Metz, L. Began: Boundary equilibrium generative adversarial networks. In *arXiv preprint arXiv:1703.10717*, 2017.

Bishop, C. M. *Pattern recognition and machine learning*. Springer, 2006.

Cissé, M., Bojanowski, P., Grave, E., Dauphin, Y., and Usunier, N. Parseval networks: Improving robustness to adversarial examples. In *International Conference on Machine Learning (ICML)*, pp. 854–863. PMLR, 2017.

Devroye, L., Györfi, L., and Lugosi, G. *A Probabilistic Theory of Pattern Recognition*. Springer Science & Business Media, 1996.

Dudley, R. M. *Real Analysis and Probability*. Cambridge Studies in Advanced Mathematics. Cambridge University Press, 2 edition, 2002a.

Dudley, R. M. *Real Analysis and Probability*. Cambridge University Press, 2002b.

Fukunaga, K. *Introduction to Statistical Pattern Recognition*. Academic press, 2013.

Goodfellow, I. J., Pouget-Abadie, J., Mirza, M., Xu, B., Warde-Farley, D., Ozair, S., Courville, A., and Bengio, Y. Generative Adversarial Nets. In *Advances in Neural Information Processing Systems (NeurIPS)*, volume 27, 2014.

Gulrajani, I., Ahmed, F., Arjovsky, M., Dumoulin, V., and Courville, A. Improved training of Wasserstein GANs. In *Advances in Neural Information Processing Systems (NeurIPS)*, volume 30, 2017.

Heusel, M., Ramsauer, H., Unterthiner, T., Nessler, B., and Hochreiter, S. GANs trained by a two time-scale update rule converge to a local nash equilibrium. In *Advances in Neural Information Processing Systems (NeurIPS)*, volume 30, 2017.

Karras, T., Aila, T., Laine, S., and Lehtinen, J. Progressive growing of gans for improved quality, stability, and variation. *arXiv preprint arXiv:1710.10196*, 2018.

Kodali, N., Abernethy, J., Hays, J., and Kira, Z. On convergence and stability of gans. In *arXiv preprint arXiv:1705.07215*, 2017.

Kynkänniemi, T., Karras, T., Laine, S., Lehtinen, J., and Aila, T. Improved precision and recall metric for assessing generative models. In *Advances in Neural Information Processing Systems*, 2019.

Lu, J., Shen, Z., Yang, H., and Zhang, S. Deep network approximation for smooth functions. *SIAM Journal on Mathematical Analysis*, 52(6):5465–5507, 2020.

Mao, X., Li, Q., Xie, H., Lau, R. Y., Wang, Z., and Smolley, S. P. Least squares generative adversarial networks. In *Proceedings of the IEEE International Conference on Computer Vision (ICCV)*, pp. 2794–2802, 2017.

Mescheder, L., Geiger, A., and Nowozin, S. Which training methods for gans do actually converge? In *International Conference on Machine Learning (ICML)*, pp. 3481–3490. PMLR, 2018.

Miyato, T., Kataoka, T., Koyama, M., and Yoshida, Y. Spectral normalization for generative adversarial networks. In *International Conference on Learning Representations (ICLR)*, 2018.

Moon, K. R., Sricharan, K., and Hero III, A. O. Ensemble estimation of distributional functionals via k -nearest neighbors. *arXiv preprint arXiv:1707.03083*, 2017.

Naeini, M. T., Bereyhi, A., Noshad, M., Liang, B., and Hero, A. O. Universal training of neural networks to achieve Bayes Optimal Classification Accuracy. In *IEEE International Conference on Acoustics, Speech and Signal Processing (ICASSP)*, pp. 1–5, 2025. doi: 10.1109/ICASSP49660.2025.10890777.

Noshad, M., Xu, L., and Hero, A. Learning to benchmark: Determining best achievable misclassification error from training data. *arXiv preprint arXiv:1909.07192*, 2019.

Nowozin, S., Cseke, B., and Tomioka, R. f-gan: Training generative neural samplers using variational divergence minimization. In *Advances in Neural Information Processing Systems (NeurIPS)*, volume 29, 2016.

Petzka, H., Fischer, A., and Lukovnicov, D. On the regularization of Wasserstein GANs. In *International Conference on Learning Representations (ICLR) Workshop*, 2018.

Saatchi, Y. and Wilson, A. G. Bayesian GAN. In *Advances in Neural Information Processing Systems (NeurIPS)*, volume 30, 2017.

Seitzer, M. Pytorch-fid: Fid score for pytorch, 2020. <https://github.com/mseitzer/pytorch-fid>.

Shalev-Shwartz, S. and Ben-David, S. *Understanding Machine Learning: From Theory to Algorithms*. Cambridge University Press, Cambridge, UK, 2014. ISBN 978-1-107-05713-5. URL <https://www.cambridge.org/9781107057135>.

Villani, C. *Optimal Transport: Old and New*. Springer, 2009.

Villani, C. et al. *Optimal Transport: Old and New*, volume 338. Grundlehren der mathematischen Wissenschaften, Springer, Berlin, Germany, 2009.

Ye, N. and Zhu, Z. Bayesian Adversarial Learning. In *Advances in Neural Information Processing Systems (NeurIPS)*, volume 31, 2018.

Zhang, C., Bengio, S., Hardt, M., Recht, B., and Vinyals, O. Understanding deep learning (still) requires rethinking generalization. *Communications of the ACM*, 64(3):107–115, 2021.

A Definitions and Preliminaries

A.1 Metrics

We recall the total variation (TV) distance and the Wasserstein- p distance, together with basic equivalences used in our analysis.

Definition 3 (Total variation). *Let P and Q be probability measures on a measurable space $(\mathcal{X}, \mathcal{F})$. The total variation distance is*

$$\text{TV}(P, Q) := \sup_{A \in \mathcal{F}} |P(A) - Q(A)|. \quad (50)$$

The total variation can be computed by equivalent forms. The following lemma gives two equivalent expressions for it.

Lemma 3 (Equivalent forms of total variation (Dudley, 2002b)). *For probability measures P and Q on $(\mathcal{X}, \mathcal{F})$,*

$$\text{TV}(P, Q) = \sup_{f: \mathcal{X} \rightarrow [0, 1]} (\mathbb{E}_{X \sim P}[f(X)] - \mathbb{E}_{X \sim Q}[f(X)]) \quad (51)$$

$$= \frac{1}{2} \sup_{\|g\|_\infty \leq 1} \left| \mathbb{E}_{X \sim P}[g(X)] - \mathbb{E}_{X \sim Q}[g(X)] \right|, \quad (52)$$

and if P and Q are absolutely continuous w.r.t. a σ -finite measure μ with densities p and q ,

$$\text{TV}(P, Q) = \frac{1}{2} \int_{\mathcal{X}} |p(x) - q(x)| d\mu(x). \quad (53)$$

Next, we define the Wasserstein distance.

Definition 4 (Wasserstein- p distance). *Let (\mathcal{X}, d) be a metric space and $p \in [1, \infty)$. For probability measures P and Q on \mathcal{X} with finite p -th moments, the Wasserstein- p distance is*

$$W_p(P, Q) := \left(\inf_{\gamma \in \Gamma(P, Q)} \int_{\mathcal{X} \times \mathcal{X}} d(x, y)^p d\gamma(x, y) \right)^{1/p}, \quad (54)$$

where $\Gamma(P, Q)$ is the set of couplings with marginals P and Q .

The Kantorovich–Rubinstein duality result gives an alternative expression for the Wasserstein-1 distance.

Definition 5 (Lipschitz continuity). *A function $f: (\mathcal{X}, \|\cdot\|) \rightarrow \mathbb{R}$ is said to be L -Lipschitz if*

$$|f(x) - f(y)| \leq L \|x - y\| \quad \forall x, y \in \mathcal{X}.$$

Its global Lipschitz constant is denoted

$$\text{Lip}(f) := \sup_{x \neq y} \frac{|f(x) - f(y)|}{\|x - y\|}.$$

Hence $\text{Lip}(f) \leq 1$ exactly when f is 1-Lipschitz.

Lemma 4 (Kantorovich–Rubinstein duality for W_1 (Villani et al., 2009)). *On a Polish metric space (\mathcal{X}, d) , for probability measures P, Q with finite first moments,*

$$W_1(P, Q) = \sup_{\text{Lip}(f) \leq 1} (\mathbb{E}_{X \sim P}[f(X)] - \mathbb{E}_{Y \sim Q}[f(Y)]), \quad (55)$$

where $\text{Lip}(f) \leq 1$ means $|f(x) - f(y)| \leq d(x, y)$ for all $x, y \in \mathcal{X}$.

In general, the total variation is a stronger notion of distance in the probability space. This can be observed from the following result.

Lemma 5 (Bounding W_1 by TV on bounded spaces (Villani et al., 2009)). *If (\mathcal{X}, d) has finite diameter $D := \sup_{x,y} d(x, y) < \infty$, then for all probability measures P and Q ,*

$$W_1(P, Q) \leq D \text{TV}(P, Q). \quad (56)$$

Sketch. By Lemma 4, scale any 1-Lipschitz f to $\tilde{f} \in [0, D]$ and apply (51).

A.2 BOLT and BOLT-GAN

Throughout, we use the following functional objectives. These objectives match the definitions given in the main paper (see Sec. 3).

Definition 6 (BOLT functional). *For a measurable $h : \mathcal{X} \rightarrow [0, 1]$, define*

$$\mathcal{L}_{\text{BOLT}}(h) := q_1 + q_2 \mathbb{E}_{X \sim P_2}[h(X)] - q_1 \mathbb{E}_{X \sim P_1}[h(X)]. \quad (57)$$

The universal bound implies that for any such h ,

$$\varepsilon_{\text{Bayes}} \leq \mathcal{L}_{\text{BOLT}}(h). \quad (58)$$

Risk and per-example BOLT loss. Let $Y \in \{1, 2\}$, $X \mid (Y = i) \sim P_i$, and let $h : \mathcal{X} \rightarrow [0, 1]$ be measurable. Define

$$s(y) := \mathbf{1}\{y = 2\} - \mathbf{1}\{y = 1\} \in \{-1, +1\}, \quad (59)$$

and the per-example loss and population risk by

$$\ell_{\text{BOLT}}(z, y) := s(y) z, \quad (60)$$

$$R(h) := \mathbb{E}[\ell_{\text{BOLT}}(h(X), Y)] = -q_1 \mathbb{E}_{X \sim P_1}[h(X)] + q_2 \mathbb{E}_{X \sim P_2}[h(X)]. \quad (61)$$

With (57),

$$\mathcal{L}_{\text{BOLT}}(h) = q_1 + R(h), \quad (62)$$

so minimizers of $R(h)$ coincide with minimizers of $\mathcal{L}_{\text{BOLT}}(h)$.

Definition 7 (Prior-weighted GAN/BOLT-GAN functional). *Let g be a generator inducing P_g , and let $h : \mathcal{X} \rightarrow [0, 1]$ be a bounded critic. For prior $\pi \in (0, 1)$,*

$$\mathcal{L}_{\text{BG}}^{(\pi)}(g, h) := \pi \mathbb{E}_{X \sim P_{\text{data}}}[h(X)] - (1 - \pi) \mathbb{E}_{X \sim P_g}[h(X)]. \quad (63)$$

It is worth mentioning that $\mathcal{L}_{\text{BG}}^{(\pi)}(g, h)$ satisfies the complementary-sum identity

$$\mathcal{L}_{\text{BG}}^{(\pi)}(g, h) + \mathcal{L}_{\text{BG}}^{(1-\pi)}(g, h) = \mathbb{E}_{X \sim P_{\text{data}}}[h(X)] - \mathbb{E}_{X \sim P_g}[h(X)]. \quad (64)$$

This is used repeatedly in our analysis to connect the BOLT-GAN objective to the TV and Wasserstein distance (see Secs. 3.2–3.3 of the main paper).

B Proofs and Further Results on BOLT

In this section we restate the result on the BOLT-assisted estimator of MAP classifier given in the main paper and provide a complete proof.

Theorem 6 (BOLT estimator of MAP classifier). *Let (X, Y) describe a binary classification problem with $Y \in \{1, 2\}$, priors $q_1 = \Pr\{Y = 1\}$ and $q_2 = \Pr\{Y = 2\} = 1 - q_1$, class-conditional laws $X \mid (Y = i) \sim P_i$, and posterior*

$$\eta(x) := \Pr\{Y = 1 \mid X = x\}. \quad (65)$$

Consider the BOLT upper bound in the $[0, 1]$ normalization (as in the main paper): for measurable $h : \mathcal{X} \rightarrow [0, 1]$ define

$$\mathcal{B}(h) := q_1 + q_2 \mathbb{E}_{X \sim P_2}[h(X)] - q_1 \mathbb{E}_{X \sim P_1}[h(X)]. \quad (66)$$

Let $h^* \in \arg \min_{h: \mathcal{X} \rightarrow [0, 1]} \mathcal{B}(h)$. Then h^* is pointwise optimal almost surely and satisfies, for $(P_1 + P_2)$ -a.e. x ,

$$h^*(x) = \begin{cases} 1, & \eta(x) > \frac{1}{2}, \\ 0, & \eta(x) < \frac{1}{2}, \\ \text{any } z \in [0, 1], & \eta(x) = \frac{1}{2}. \end{cases} \quad (67)$$

Consequently, the plug-in classifier at threshold $1/2$,

$$\widehat{C}(x) = \mathbf{1}\{h^*(x) \geq \frac{1}{2}\}, \quad (68)$$

coincides almost everywhere with the MAP decision rule $\mathbf{1}\{\eta(x) \geq \frac{1}{2}\}$.

Moreover, if a learned model h_θ satisfies $\|h_\theta - h^*\|_\infty \leq \varepsilon$ for some $\varepsilon < \frac{1}{2}$, then the plug-in decision

$$\widehat{C}_\theta(x) = \mathbf{1}\{h_\theta(x) \geq \frac{1}{2}\} \quad (69)$$

agrees with $\widehat{C}(x)$ (and hence with MAP) except possibly on the decision boundary set $\{x : \eta(x) = \frac{1}{2}\}$.

Proof. The additive constant q_1 does not affect minimizers, so minimizing $\mathcal{B}(h)$ over h is equivalent to minimizing

$$R(h) := q_2 \mathbb{E}_{X \sim P_2}[h(X)] - q_1 \mathbb{E}_{X \sim P_1}[h(X)]. \quad (70)$$

Fix $x \in \mathcal{X}$ and abbreviate $\eta = \eta(x)$. The conditional risk of predicting a value $z \in [0, 1]$ is

$$\begin{aligned} r_\eta(z) &:= \mathbb{E}[\ell(z, Y) \mid X = x] \\ &= \eta \ell(z, 1) + (1 - \eta) \ell(z, 2), \end{aligned} \quad (71)$$

where (consistent with the main text) $\ell(z, 1) = -z$ and $\ell(z, 2) = +z$. Hence

$$\begin{aligned} r_\eta(z) &= \eta(-z) + (1 - \eta)z \\ &= (1 - 2\eta)z. \end{aligned} \quad (72)$$

To minimize $r_\eta(z)$ over $z \in [0, 1]$:

- If $\eta > \frac{1}{2}$ then $1 - 2\eta < 0$ and $r_\eta(z)$ is decreasing in z , so the minimum is at $z = 1$.
- If $\eta < \frac{1}{2}$ then $1 - 2\eta > 0$ and $r_\eta(z)$ is increasing in z , so the minimum is at $z = 0$.
- If $\eta = \frac{1}{2}$ then $r_\eta(z) \equiv 0$ and any $z \in [0, 1]$ is optimal.

This yields the pointwise characterization (67).

For the plug-in rule, when $\eta(x) \neq \frac{1}{2}$ we have $h^*(x) \in \{0, 1\}$, and

$$h^*(x) \geq \frac{1}{2} \iff h^*(x) = 1 \iff \eta(x) > \frac{1}{2}, \quad (73)$$

so (68) agrees with MAP almost everywhere (ties only when $\eta(x) = \frac{1}{2}$).

Finally, if $\|h_\theta - h^*\|_\infty \leq \varepsilon < \frac{1}{2}$ and $h^*(x) \in \{0, 1\}$, then $h_\theta(x)$ cannot cross the threshold $1/2$, so (69) matches (68) away from the boundary set $\{\eta = \frac{1}{2}\}$. \square

Corollary 3 (Bayes consistency of the plug-in classifier). *Assume*

$$\Pr\left(\eta(X) = \frac{1}{2}\right) = 0, \quad (74)$$

under the distribution of (X, Y) , where $\eta(x) = \Pr\{Y = 1 \mid X = x\}$. Let $\hat{h}_n : \mathcal{X} \rightarrow [0, 1]$ be risk-consistent for the BOLT loss $\ell(z, 1) = -z$ and $\ell(z, 2) = +z$, i.e.

$$R(\hat{h}_n) \xrightarrow{n \rightarrow \infty} \inf_{h: \mathcal{X} \rightarrow [0, 1]} R(h) = R(h^*), \quad (75)$$

where

$$R(h) := \mathbb{E}[\ell(h(X), Y)] = -q_1 \mathbb{E}_{X \sim P_1}[h(X)] + q_2 \mathbb{E}_{X \sim P_2}[h(X)]. \quad (76)$$

Define the plug-in classifier at threshold 1/2,

$$\hat{C}_n(x) := \mathbf{1}\left\{\hat{h}_n(x) \geq \frac{1}{2}\right\}. \quad (77)$$

Then the 0-1 risk converges to the Bayes risk:

$$\Pr\left(\hat{C}_n(X) \neq Y\right) \xrightarrow{n \rightarrow \infty} \Pr(C_{\text{MAP}}(X) \neq Y). \quad (78)$$

Proof. Let h^* be a population minimizer from Theorem 6 (your $[0, 1]$ version), so $h^*(x) \in \{0, 1\}$ for $\eta(x) \neq \frac{1}{2}$. Fix $x \in \mathcal{X}$ and abbreviate $\eta = \eta(x)$. The conditional risk of predicting $z \in [0, 1]$ is

$$r_\eta(z) := \mathbb{E}[\ell(z, Y) \mid X = x] = \eta(-z) + (1 - \eta)z = (1 - 2\eta)z. \quad (79)$$

As in Theorem 6, $z^* \in \arg \min_{z \in [0, 1]} r_\eta(z)$ satisfies $z^* = 1$ if $\eta > \frac{1}{2}$, $z^* = 0$ if $\eta < \frac{1}{2}$, and any $z^* \in [0, 1]$ if $\eta = \frac{1}{2}$. Hence, for any $\hat{z} \in [0, 1]$,

$$r_\eta(\hat{z}) - r_\eta(z^*) = |1 - 2\eta| \cdot |\hat{z} - z^*|. \quad (80)$$

Taking expectation over X gives

$$R(\hat{h}_n) - R(h^*) = \mathbb{E}\left[|1 - 2\eta(X)| |\hat{h}_n(X) - h^*(X)|\right] \xrightarrow{n \rightarrow \infty} 0. \quad (81)$$

Let $E_n := \{\hat{C}_n(X) \neq C_{\text{MAP}}(X)\}$. For any $\delta \in (0, 1)$,

$$E_n \subseteq \left(E_n \cap \{|1 - 2\eta(X)| \geq \delta\}\right) \cup \{|1 - 2\eta(X)| < \delta\}. \quad (82)$$

On the event $\{|1 - 2\eta(X)| \geq \delta\}$, a decision mismatch (threshold 1/2) implies $|\hat{h}_n(X) - h^*(X)| \geq \frac{1}{2}$ because $h^*(X) \in \{0, 1\}$ there. Therefore,

$$\begin{aligned} R(\hat{h}_n) - R(h^*) &\geq \mathbb{E}\left[|1 - 2\eta(X)| \cdot |\hat{h}_n(X) - h^*(X)| \cdot \mathbf{1}_{E_n \cap \{|1 - 2\eta(X)| \geq \delta\}}\right] \\ &\geq \frac{\delta}{2} \Pr(E_n \cap \{|1 - 2\eta(X)| \geq \delta\}). \end{aligned} \quad (83)$$

Sending $n \rightarrow \infty$ and using (81) yields

$$\Pr(E_n \cap \{|1 - 2\eta(X)| \geq \delta\}) \xrightarrow{n \rightarrow \infty} 0. \quad (84)$$

Moreover, by (74), $\Pr(|1 - 2\eta(X)| < \delta) \rightarrow 0$ as $\delta \downarrow 0$. Combining this with (82) proves that $\Pr(E_n) \rightarrow 0$, i.e. $\hat{C}_n(X)$ agrees with $C_{\text{MAP}}(X)$ with probability tending to 1. This implies the 0-1 risk convergence (78). \square

B.1 Bias and Variance of BOLT

This subsection provides the full statements and proofs corresponding to **Remark 3** in the main paper. We analyze the BOLT loss via plug-in estimators of the likelihood ratio together with a hinge map. The key structural fact is that the population optimizer of the BOLT bound is a hinge of the likelihood ratio; hence optimizing $h(\cdot)$ amounts to estimating $U(x)$, and errors in h mirror errors in U .

Setup and Notation Let (X, C) be binary with classes $C \in \{C_1, C_2\}$, priors $q_i = \Pr\{C = C_i\} > 0$ with $q_1 + q_2 = 1$, and conditionals $X \mid (C = C_i) \sim P_i$ (densities p_i). Define the likelihood ratio $U(x)$ and the prior threshold τ as

$$U(x) := \frac{p_1(x)}{p_2(x)}, \quad \tau := \frac{q_2}{q_1}. \quad (85)$$

Theorem 7 (Optimal bounding function and tightness). *Assume $q_1, q_2 > 0$ and that P_1, P_2 admit densities p_1, p_2 w.r.t. a common dominating measure. Define*

$$U(x) := \frac{p_1(x)}{p_2(x)} \quad \text{on } \{p_2(x) > 0\}, \quad \tau := \frac{q_2}{q_1}, \quad (86)$$

and let

$$c(x) := q_1 p_1(x) - q_2 p_2(x). \quad (87)$$

A pointwise maximizer of $c(x)h(x)$ over $h(x) \in [0, 1]$ is

$$h^*(x) = \begin{cases} 0, & U(x) < \tau, \\ 1, & U(x) \geq \tau, \end{cases} \quad (88)$$

and the BOLT bound is tight:

$$\mathcal{L}_{\text{BOLT}}(h^*) = \varepsilon_{\text{Bayes}}, \quad (89)$$

where (consistent with Def. 6)

$$\mathcal{L}_{\text{BOLT}}(h) := q_1 + q_2 \mathbb{E}_{X \sim P_2}[h(X)] - q_1 \mathbb{E}_{X \sim P_1}[h(X)]. \quad (90)$$

Proof. **Endpoint optimality.** For fixed x , the map $h \mapsto c(x)h$ is affine on $[0, 1]$, hence maximized at an endpoint chosen by the sign of $c(x)$: $h^*(x) = 1$ if $c(x) \geq 0$ and $h^*(x) = 0$ if $c(x) < 0$. Since $c(x) < 0$ holds if and only if $q_1 p_1(x) < q_2 p_2(x)$, i.e. $U(x) < \tau$, we obtain (88).

Tightness. Using the definition (90) and substituting h^* , we have

$$\mathcal{L}_{\text{BOLT}}(h^*) = q_1 + q_2 \mathbb{E}_{X \sim P_2}[h^*(X)] - q_1 \mathbb{E}_{X \sim P_1}[h^*(X)] \quad (91)$$

$$= q_1 + \int (q_2 p_2(x) - q_1 p_1(x)) h^*(x) dx \quad (92)$$

$$= q_1 + \int (q_2 p_2(x) - q_1 p_1(x)) \mathbf{1}\{U(x) \geq \tau\} dx \quad (93)$$

$$= q_1 - \int (q_1 p_1(x) - q_2 p_2(x)) \mathbf{1}\{U(x) \geq \tau\} dx \quad (94)$$

$$= q_1 - \int [q_1 p_1(x) - q_2 p_2(x)]_+ dx \quad (95)$$

$$= q_1 - \int (\max\{q_1 p_1(x), q_2 p_2(x)\} - q_2 p_2(x)) dx \quad (96)$$

$$= q_1 - \int \max\{q_1 p_1(x), q_2 p_2(x)\} dx + \int q_2 p_2(x) dx \quad (97)$$

$$= 1 - \int \max\{q_1 p_1(x), q_2 p_2(x)\} dx = \varepsilon_{\text{Bayes}}. \quad (98)$$

Here we used $[a]_+ = a \mathbf{1}\{a > 0\}$ and the identity $[b - a]_+ = \max\{b, a\} - a$ (with $b = q_1 p_1(x)$, $a = q_2 p_2(x)$), and also $\int q_2 p_2(x) dx = q_2$. This completes the proof. \square

The above result gives an interesting connection between the Bayes error and the likelihood ratio.

Corollary 4 (Bayes error as a hinge of the likelihood ratio). *Define the hinge map*

$$t_0(u) := [q_2 - q_1 u]_+. \quad (99)$$

Then the Bayes error rate is given by

$$\varepsilon_{\text{Bayes}} = q_2 - \mathbb{E}_{X \sim P_2} [t_0(U(X))]. \quad (100)$$

Proof. Recall

$$\varepsilon_{\text{Bayes}} = 1 - \int \max\{q_1 p_1(x), q_2 p_2(x)\} dx = \int \min\{q_1 p_1(x), q_2 p_2(x)\} dx. \quad (101)$$

Using $\min\{a, b\} = b - [b - a]_+$ with $a = q_1 p_1(x)$ and $b = q_2 p_2(x)$, we get

$$\begin{aligned} \varepsilon_{\text{Bayes}} &= \int q_2 p_2(x) dx - \int [q_2 p_2(x) - q_1 p_1(x)]_+ dx \\ &= q_2 - \int p_2(x) [q_2 - q_1 U(x)]_+ dx = q_2 - \mathbb{E}_{X \sim P_2} [q_2 - q_1 U(X)]_+, \end{aligned} \quad (102)$$

which is (100). \square

Plug-in estimator (empirical context). Suppose we observe M_1 samples from class C_1 and M_2 from class C_2 (with total $M = M_1 + M_2$), and set empirical priors

$$\hat{q}_i := \frac{M_i}{M}, \quad i \in \{1, 2\}. \quad (103)$$

Let \hat{U} estimate U , and let $X_1^{(2)}, \dots, X_{M_2}^{(2)}$ $\stackrel{\text{i.i.d.}}{\sim} P_2$ be the M_2 samples of class- C_2 used to estimate the expectation over P_2 in (100). Define

$$\hat{t}_0(u) := [\hat{q}_2 - \hat{q}_1 u]_+, \quad \hat{\varepsilon}_{\text{BOLT}} := \hat{q}_2 - \frac{1}{M_2} \sum_{i=1}^{M_2} \hat{t}_0(\hat{U}(X_i^{(2)})). \quad (104)$$

Note that $0 \leq t_0(u) \leq q_2 \leq 1$ and $0 \leq \hat{t}_0(u) \leq \hat{q}_2 \leq 1$, so all summands are bounded in $[0, 1]$.

Lemma 6 (Lipschitz property of the hinge). *The map $t_0(u) = [q_2 - q_1 u]_+$ is globally q_1 -Lipschitz:*

$$|t_0(u) - t_0(v)| \leq q_1 |u - v| \quad \forall u, v \in \mathbb{R}. \quad (105)$$

Proof. Let $\tau = q_2/q_1$. If $u, v \leq \tau$, then t_0 is affine with slope $-q_1$, giving equality in (105). If $u, v \geq \tau$, both values are 0. If $u \leq \tau \leq v$ (or vice versa), then $t_0(u) - t_0(v) = t_0(u) = q_2 - q_1 u \leq q_1(\tau - u) \leq q_1|u - v|$. \square

Theorem 8 (Bias and variance of the binary BOLT plug-in estimator). *Assume i.i.d. draws and bounded hinge summands in $[0, 1]$. Then*

$$|\mathbb{E}[\hat{\varepsilon}_{\text{BOLT}}] - \varepsilon_{\text{Bayes}}| \leq q_1 \mathbb{E}_{X \sim P_2} [|\hat{U}(X) - U(X)|] + O(M^{-1/2}), \quad (106)$$

$$\text{Var}(\hat{\varepsilon}_{\text{BOLT}}) = O(M^{-1}). \quad (107)$$

In particular, if $\mathbb{E}_{X \sim P_2} [|\hat{U}(X) - U(X)|] \leq \varepsilon_0$, then

$$|\mathbb{E}[\hat{\varepsilon}_{\text{BOLT}}] - \varepsilon_{\text{Bayes}}| \leq q_1 \varepsilon_0 + O(M^{-1/2}). \quad (108)$$

Proof. Bias. By (104) and adding/subtracting $\mathbb{E}_{X \sim P_2} [t_0(\hat{U}(X))]$, we have

$$\mathbb{E}[\hat{\varepsilon}_{\text{BOLT}}] - \varepsilon_{\text{Bayes}} = \underbrace{\mathbb{E}_{X \sim P_2} [t_0(U(X)) - t_0(\hat{U}(X))]}_{\text{plug-in error}} + \underbrace{\mathbb{E} \left[\mathbb{E}_{X \sim P_2} [t_0(\hat{U}(X))] - \frac{1}{M_2} \sum_{i=1}^{M_2} \hat{t}_0(\hat{U}(X_i^{(2)})) \right]}_{\text{sampling/priors}}. \quad (109)$$

By Lemma 6, t_0 is q_1 -Lipschitz, so

$$\left| \mathbb{E}_{X \sim P_2} [t_0(U(X)) - t_0(\widehat{U}(X))] \right| \leq q_1 \mathbb{E}_{X \sim P_2} [|\widehat{U}(X) - U(X)|]. \quad (110)$$

For the sampling/priors term, write $Z_i = \widehat{t}_0(\widehat{U}(X_i^{(2)})) \in [0, 1]$. Hoeffding implies $\mathbb{E} \left| \frac{1}{M_2} \sum_{i=1}^{M_2} Z_i - \mathbb{E} Z_1 \right| = O(M_2^{-1/2})$. The empirical priors $\widehat{q}_i = M_i/M$ add a zero-mean fluctuation with variance $O(M^{-1})$, hence $O(M^{-1/2})$ in expectation. With fixed class proportions ($M_2 = \Theta(M)$), these contributions yield (106).

Variance. Using $\widehat{\varepsilon}_{\text{BOLT}} = \widehat{q}_2 - \frac{1}{M_2} \sum_{i=1}^{M_2} Z_i$ with bounded Z_i , $\text{Var}(\frac{1}{M_2} \sum_i Z_i) = O(M_2^{-1})$ and $\text{Var}(\widehat{q}_2) = O(M^{-1})$. Any covariance between these two bounded averages is $O(M^{-1})$, hence (107). \square

Remark 1 (Typical rates for ε_0). *We bundle approximation and estimation errors into $\varepsilon_0 := \varepsilon_{\text{approx}} + \varepsilon_{\text{est}}$. Under standard smoothness/capacity assumptions,*

$$\varepsilon_0 = O(W^{-\gamma} + N^{-1/2}),$$

where W is a width/capacity proxy, N is the number of training samples used to learn \widehat{U} , and $\gamma > 0$ depends on the target smoothness and the approximating family (Lu et al., 2020; Shalev-Shwartz & Ben-David, 2014).

C Further Results on BOLT-GAN

We present additional properties of the BOLT-GAN objective and its connections to standard distances. Throughout, we use the prior-weighted functional $L_{\text{BG}}^{(\pi)}(g, h)$ as defined in the main text (Sec. 3). We do not restate it here to avoid duplication.

Basic bounds. We first preclude degenerate values when the critic is bounded.

Lemma 7 (Lower and upper bounds). *For any generator g and any bounded critic $h : \mathcal{X} \rightarrow [0, 1]$,*

$$\pi - 1 \leq L_{\text{BG}}^{(\pi)}(g, h) \leq \pi. \quad (111)$$

Both bounds are tight in the sense that there exists a pair (g, h) attaining them.

Proof. Since $0 \leq \mathbb{E}_{P_{\text{data}}}[h] \leq 1$ and $0 \leq \mathbb{E}_{P_g}[h] \leq 1$, $L_{\text{BG}}^{(\pi)}(g, h) = \pi \mathbb{E}_{P_{\text{data}}}[h] - (1 - \pi) \mathbb{E}_{P_g}[h] \in [\pi - 1, \pi]$. Tightness follows by choosing distributions and a measurable h that separate supports: if $h = 1$ on $\text{supp}(P_{\text{data}})$ and $h = 0$ on $\text{supp}(P_g)$, the value is π ; if $h = 0$ on $\text{supp}(P_{\text{data}})$ and $h = 1$ on $\text{supp}(P_g)$, it is $\pi - 1$. \square

Monotonicity in the prior. We next show that the maximized gap grows with π .

Lemma 8 (Monotonicity in π). *Fix a generator g with density q and write p for the data density w.r.t. a common dominating measure. Let*

$$D^{(\pi)}(g) := \max_{h: \mathcal{X} \rightarrow [0, 1]} L_{\text{BG}}^{(\pi)}(g, h) = \int_{\mathcal{X}} [\pi p(x) - (1 - \pi) q(x)]_+ dx. \quad (112)$$

Then $D^{(\pi)}(g)$ is nondecreasing in $\pi \in [0, 1]$.

Proof. For each fixed x , the map $\pi \mapsto [\pi p(x) - (1 - \pi) q(x)]_+$ is nondecreasing: its derivative is $p(x) + q(x) > 0$ wherever the bracket is positive and 0 elsewhere. We obtain the desired result by integrating over \mathcal{X} . \square

Balanced vs. prior-weighted gap (Lipschitz critics). We now relate the prior-weighted objective to its “balanced” counterpart on a 1-Lipschitz class. Let:

$$\mathcal{H}_{\text{Lip}} := \{ h : \mathcal{X} \rightarrow [0, 1] : |h(x) - h(y)| \leq \|x - y\| \forall x, y \in \mathcal{X} \}, \quad (113)$$

$$D_{\text{Lip}}^{(\pi)}(g) := \pi \sup_{h \in \mathcal{H}_{\text{Lip}}} \mathbb{E}_{X \sim P_{\text{data}}}[h(X)] - (1 - \pi) \mathbb{E}_{X \sim P_g}[h(X)], \quad (114)$$

$$\Sigma_{\text{Lip}}(g) := \sup_{h \in \mathcal{H}_{\text{Lip}}} \left(\mathbb{E}_{X \sim P_{\text{data}}}[h(X)] - \mathbb{E}_{X \sim P_g}[h(X)] \right). \quad (115)$$

The next inequality is the pointwise scalar comparison we use repeatedly.

Lemma 9 (Pointwise dominance). *For $0 < \pi \leq \frac{1}{2}$ and any $a, b \in [0, 1]$,*

$$\max\{a - b, b - a\} \geq \pi a - (1 - \pi) b. \quad (116)$$

Proof. If $a \geq b$, then

$$(a - b) - (\pi a - (1 - \pi) b) = (1 - \pi)a - \pi b \geq (1 - \pi)b - \pi b = (1 - 2\pi)b \geq 0.$$

If $a < b$, the claim is equivalent to

$$(b - a) - (\pi a - (1 - \pi) b) = (2 - \pi)b - (1 + \pi)a \geq 0,$$

which holds since $a \leq b$ and $(2 - \pi)/(1 + \pi) \geq 1$ for $\pi \leq \frac{1}{2}$. \square

Proposition 1 (From pointwise to functional dominance). *For $0 < \pi \leq \frac{1}{2}$,*

$$D_{\text{Lip}}^{(\pi)}(g) \leq \Sigma_{\text{Lip}}(g). \quad (117)$$

Proof. For any $h \in \mathcal{H}_{\text{Lip}}$, write $a = \mathbb{E}_{P_{\text{data}}}[h]$ and $b = \mathbb{E}_{P_g}[h]$. By Lemma 9, $\max\{a - b, b - a\} \geq \pi a - (1 - \pi) b$. Since $h \mapsto 1 - h$ preserves \mathcal{H}_{Lip} and flips $a - b$ to $b - a$,

$$\sup_{h \in \mathcal{H}_{\text{Lip}}} \max\{a - b, b - a\} = \sup_{h \in \mathcal{H}_{\text{Lip}}} (a - b) = \Sigma_{\text{Lip}}(g).$$

Taking suprema on both sides over $h \in \mathcal{H}_{\text{Lip}}$ yields the claim. \square

Bridge to W_1 (pointer). Combining Proposition 1 with the complementary-sum identity from the main paper and the Kantorovich–Rubinstein dual (sup over all 1-Lipschitz functions without range constraints) gives the bound $D_{\text{Lip}}^{(\pi)}(g) \leq W_1(P_{\text{data}}, P_g)$ used in the main text. We omit the re-statement here to avoid duplication.

Role of the basic bound (Lemma 7). Together with the balanced-sum identity in the paper (Sec. 3), Lemma 7 ensures that each prior-weighted term is uniformly bounded when $h \in [0, 1]$, preventing pathological cancellations when one passes to the balanced form in intermediate maximizations.

Symmetry for $\pi > \frac{1}{2}$. The case $\pi > \frac{1}{2}$ follows by exchanging labels (replacing π with $1 - \pi$, i.e., swapping P_{data} and P_g). Thus the conclusions above extend to all $\pi \in (0, 1]$ by symmetry.

In summary, for $0 < \pi \leq 1$,

$$D_{\text{Lip}}^{(\pi)}(g) \leq \Sigma_{\text{Lip}}(g) \leq W_1(P_{\text{data}}, P_g),$$

This is precisely the inequality chain invoked in the proof of the Lipschitz BOLT–GAN result in the main paper.

D Implementation of Lipschitz BOLT-GAN

This section records the implementation details for our Lipschitz BOLT-GAN experiments. We explain the properties we rely on and the techniques used to enforce the 1-Lipschitz constraint on the discriminator (critic). As discussed in the main paper, Lipschitz continuity is key both (i) to recover meaningful dual objectives (e.g., the KR dual for W_1) and (ii) to stabilize adversarial training; see the TV/Wasserstein connections in Secs. 3.2–3.3. In our code, the gradient penalty is applied to the *raw* critic output \tilde{h}_θ (pre-activation), and the bounded score $h_\theta = \sigma(\tilde{h}_\theta) \in [0, 1]$ is used inside the BOLT objective, as summarized in Algorithm 1. (Gulrajani et al., 2017; Miyato et al., 2018, Sec. 3).

D.1 Preliminaries on Lipschitz continuity

Lemma 10 (Basic Lipschitz calculus (Miyato et al., 2018)). *Let f, g, f_1 , and f_2 be Lipschitz. Then*

$$\text{Lip}(g \circ f) \leq \text{Lip}(g) \text{Lip}(f), \quad (118)$$

$$\text{Lip}(f_1 + f_2) \leq \text{Lip}(f_1) + \text{Lip}(f_2). \quad (119)$$

Lemma 11 (Layerwise Lipschitz constants in common architectures (Miyato et al., 2018; Anil et al., 2019)). *Assume all vector spaces are equipped with the Euclidean norm $\|\cdot\|_2$, and for a function f we write $\text{Lip}(f)$ for its global Lipschitz constant with respect to $\|\cdot\|_2$.*

(i) **Linear / convolutional layers.** *For an affine map $T(x) = Wx + b$ (fully connected) or a convolutional layer viewed as a linear map $x \mapsto Wx$,*

$$\text{Lip}(T) = \|W\|_2,$$

i.e., the operator (spectral) norm of W . Biases do not affect Lip .

(ii) **Pointwise activations (elementwise maps).** *If ϕ is applied elementwise, then $\text{Lip}(\phi) = \sup_{t \in \mathbb{R}} |\phi'(t)|$ (when the derivative exists a.e.).*

(iii) **Residual blocks.** *For a residual block of the form $x \mapsto Sx + F(x)$ with a linear skip S (identity or 1×1 projection),*

$$\text{Lip}(x \mapsto Sx + F(x)) \leq \|S\|_2 + \text{Lip}(F).$$

In particular, if $S = I$, then $\text{Lip} \leq 1 + \text{Lip}(F)$.

(iv) **Resampling operators.** *If S is a (linear) down/up-sampling operator used before or after a block F , then*

$$\text{Lip}(F \circ S) \leq \text{Lip}(F) \|S\|_2, \quad \text{Lip}(S \circ F) \leq \|S\|_2 \text{Lip}(F).$$

Common strided convolutions, pooling, and interpolation are linear maps with finite $\|S\|_2$ that must be accounted for in per-layer bounds.

Remark 2 (Standard elementwise activations and their Lip). *The following are explicit formulas for common activations used in (ii), together with their Lipschitz constants:*

$$\text{ReLU}(t) = \max\{0, t\}, \quad \text{Lip} = 1; \quad \tanh(t) = \frac{e^t - e^{-t}}{e^t + e^{-t}}, \quad \text{Lip} = 1;$$

$$\text{LeakyReLU}_\alpha(t) = \begin{cases} t, & t \geq 0 \\ \alpha t, & t < 0 \end{cases}, \quad \text{Lip} = \max\{1, \alpha\}; \quad \sigma(t) = \frac{1}{1 + e^{-t}}, \quad \sigma'(t) = \sigma(t)(1 - \sigma(t)) \leq \frac{1}{4}, \quad \text{Lip} = \frac{1}{4}.$$

D.2 Spectral Normalization (SN)

Method. Each linear layer W is rescaled by an estimate of its top singular value $\sigma(W)$ via power iteration with persistent vectors (u, v) : $\tilde{W} \leftarrow W/\sigma(W)$. For convolutions, $\sigma(W)$ is the operator norm of the induced linear map and can be estimated by alternating conv/transpose-conv passes. (Miyato et al., 2018).

Guarantee. If every linear/convolutional layer is normalized so that $\|W\|_2 \leq 1$ and all activations are 1-Lipschitz, then by Lemmas 10–11 the whole network is 1-Lipschitz (up to residual additions; see “Residual blocks” below). This yields strong stability at low computational cost and is widely adopted in GAN critics. (Miyato et al., 2018).

Residual blocks and skips. Because $\text{Lip}(x + F(x)) \leq 1 + \text{Lip}(F)$, residual connections can increase the global constant above 1. Two common remedies are: (i) apply SN to the skip 1×1 projection; (ii) scale residual branches by $c < 1$ (“residual scaling”) to keep $\text{Lip}(F) \leq c$, so the block is $\leq 1 + c$.

D.3 Gradient Penalty (GP)

Method. Gradient penalty encourages $\|\nabla_x \tilde{h}_\theta(x)\|_2 \approx 1$ on a chosen sampling distribution. The most common choice is the *interpolation penalty* (Gulrajani et al., 2017): draw $(x_{\text{real}}, x_{\text{fake}})$, form $\hat{x} = \alpha x_{\text{real}} + (1 - \alpha)x_{\text{fake}}$ with $\alpha \sim \text{Unif}[0, 1]$, and add

$$\lambda \mathbb{E}_{\hat{x}} (\|\nabla_{\hat{x}} \tilde{h}_\theta(\hat{x})\|_2 - 1)^2 \quad (120)$$

to the critic loss. We penalize *pre-activation* \tilde{h}_θ , not $\sigma(\tilde{h}_\theta)$, to avoid shrinking gradients through the 1/4-Lipschitz sigmoid.

Guarantee (local, not global). The penalty (120) is a *soft* constraint: it is zero iff the gradient norm equals 1 on the support where it is evaluated (here, segments between real/fake samples). It does not by itself prove a *global* 1-Lipschitz bound, but it aligns with the KR optimal-critic condition and markedly improves training stability. (Gulrajani et al., 2017).

Implementation notes.

- *Backprop through the norm.* Ensure gradients flow through $\|\nabla_{\hat{x}} \tilde{h}_\theta(\hat{x})\|_2$ (autodiff: create graph for higher-order grads).
- *Normalization.* Avoid BatchNorm in the critic; prefer layer/instance norm or none.
- *Lazy regularization.* Apply the penalty every k steps and scale $\lambda \leftarrow k\lambda$ to keep the expected contribution unchanged.
- *Tuning λ .* Start with $\lambda \in [1, 10]$ and monitor the penalty/critic ratio (see diagnostics below).

D.4 Weight clipping

Method. Clip each parameter after every update: $w \leftarrow \text{clip}(w, -L_{\text{wc}}, L_{\text{wc}})$ (Arjovsky et al., 2017). This loosely bounds per-layer operator norms via element-wise bounds.

Guarantee (coarse). If a layer $W \in \mathbb{R}^{m \times n}$ is element-wise clipped as $|W_{ij}| \leq L_{\text{wc}}$, then

$$\|W\|_2 \leq \|W\|_{\text{F}} \leq \sqrt{mn} L_{\text{wc}}, \quad (121)$$

so a depth- L network with 1-Lipschitz activations satisfies $\text{Lip}(f) \leq \prod_{\ell=1}^L \sqrt{m_\ell n_\ell} L_{\text{wc}}$. This yields at best a *coarse* global bound and often harms capacity. In practice we prefer SN or GP. (Arjovsky et al., 2017; Miyato et al., 2018).

D.5 Other gradient penalties and related methods

- **One-sided GP (Lipschitz penalty).** Penalize only $\|\nabla \tilde{h}_\theta\|_2 > 1$: $\lambda \mathbb{E}[\max(0, \|\nabla \tilde{h}_\theta\| - 1)^2]$, avoiding a push toward < 1 gradients that can reduce capacity (Petzka et al., 2018).
- **Zero-centered penalties R_1/R_2 .** Apply $\lambda \mathbb{E}_{x \sim P_{\text{data}}} \|\nabla_x \tilde{h}_\theta(x)\|_2^2$ (R_1) or $\lambda \mathbb{E}_{x \sim P_g} \|\nabla_x \tilde{h}_\theta(x)\|_2^2$ (R_2) to improve convergence empirically—even though they do not strictly enforce 1-Lipschitzness (Mescheder et al., 2018).

- **DRAGAN (local penalties).** Sample $\hat{x} = x_{\text{real}} + \delta$ with small noise and penalize $\|\nabla_{\hat{x}} \tilde{h}_{\theta}(\hat{x})\|_2$ near the data manifold to promote local smoothness (Kodali et al., 2017).
- **Orthogonal/Parseval constraints.** Constrain $W^T W \approx I$ (Parseval/Björck) to shrink $\|W\|_2$ toward 1 at higher compute cost (Cissé et al., 2017).
- **Lipschitz activations.** Using activations with known Lipschitz constants (e.g., GroupSort) can yield provably 1-Lipschitz networks when combined with spectral control of linear layers (Anil et al., 2019).
- **Optimizer-level gradient clipping.** Stabilizes updates but *does not* impose a function-level Lipschitz bound; . We emphasize that this is different from SN or GP.

These alternatives differ in how strictly they enforce the Lipschitz constraint versus how much computational cost or flexibility they introduce, and we mention them here for completeness.

D.6 Diagnostics and failure modes

We use the following techniques to keep the critic near the 1-Lipschitz regime while preserving capacity and useful gradients to the generator.

- **Monitor gradient norms.** Track the empirical distribution of $\|\nabla_{\hat{x}} \tilde{h}_{\theta}(\hat{x})\|_2$ (for \hat{x} used in the penalty). For WGAN-GP, it should concentrate near 1. Heavy mass $\gg 1$: increase λ or apply the penalty more frequently. Heavy mass $\ll 1$: reduce λ or switch to one-sided GP.
- **Penalty/critic ratio.** Log $\mathbb{E}[(\|\nabla\| - 1)^2]/\mathbb{E}[\text{critic term}]$. Ratios $\ll 10^{-2}$ indicates an ineffective penalty; $\gg 10$ indicates capacity strangling.
- **Check residual branches.** With SN, ensure skip paths are constrained (SN on 1×1 skips or residual scaling); otherwise the global constant can inflate.
- **Avoid BatchNorm in critics.** Batch-dependent statistics interact poorly with gradient penalties and can inject noise into $\|\nabla_x \tilde{h}_{\theta}\|$; use layer/instance norm or none.

E Additional Experimental Results

E.1 CelebA-64 λ_{GP} Sensitivity for BOLT-GAN

For completeness, Figure 4 presents the CelebA-64 λ_{GP} sweep mirroring the CIFAR-10 analysis in the main text. The stability/performance trends are consistent: $\lambda_{\text{GP}} \in [5, 10]$ is best, with variations within ± 1 FID.

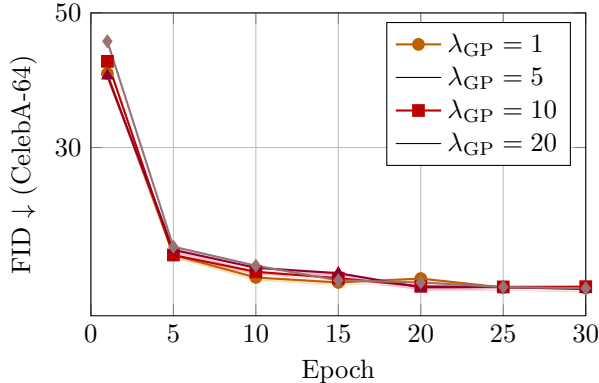


Figure 4: **BOLT-GAN-GP on CelebA-64:** FID vs. epochs for different λ_{GP} values (mean \pm std over 3 seeds). The trend mirrors CIFAR-10: near-optimal, stable performance for $\lambda_{\text{GP}} \in [5, 10]$.

E.2 Qualitative Results

We provide qualitative samples to complement the quantitative results in the main paper: each panel below shows an uncurated 4×4 grid of random images generated by BOLT-GAN-GP after 20 training epochs under the same setup as our primary experiments (same architectures, optimizer, and λ_{GP}).

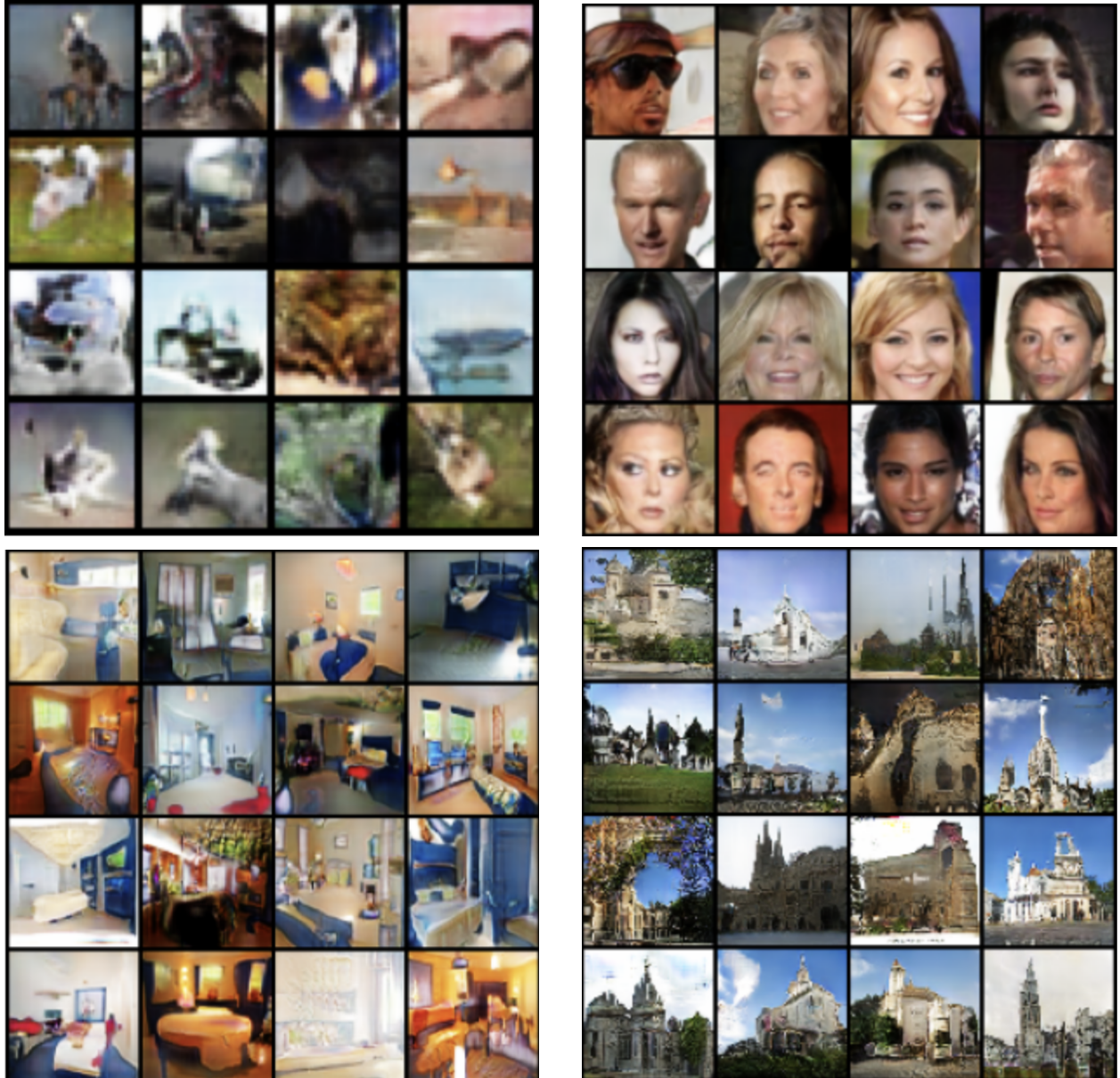


Figure 5: *Qualitative samples (first experiment of the main paper)*. BOLT-GAN-GP after 20 epochs with $\lambda_{\text{GP}}=10$. Top-left: CIFAR-10; top-right: CelebA-64; bottom-left: LSUN Bedroom-64; bottom-right: LSUN Church-64. Each panel shows the same 4×4 grid of generated samples at a reduced scale. Under the identical setup used in our main experiments, Lipschitz BOLT-GAN produces sharper textures, fewer checkerboard artifacts, and more stable color statistics than the WGAN-GP baseline.

F Implementation Details

This section records everything needed to reproduce our results, together with the rationale for each design choice and how the pieces interact (objective, Lipschitz control, optimization, and evaluation). The discriminator produces a raw scalar score $\tilde{h}_\theta(x) \in \mathbb{R}$ and a bounded score $h_\theta(x) = \sigma(\tilde{h}_\theta(x)) \in [0, 1]$ that is used in the BOLT objective. All gradient penalties are applied to the *raw* score \tilde{h}_θ .

F.1 Codebase, Environment, and Hardware

We use Python 3.10+ and the CUDA-enabled build of PyTorch. To improve throughput and reduce memory footprint without affecting FID, we enable automatic mixed precision (AMP) for both networks. When we report “deterministic” runs, we enable determinism switches so that snapshots and sample grids can be reproduced exactly, and we average metrics over multiple random seeds. All experiments were run on NVIDIA A100 GPUs.

F.2 Datasets and Preprocessing

We intentionally keep preprocessing minimal in order to maintain comparability of FID with prior work. Unless otherwise stated, we do not use data augmentation. For **CIFAR-10**, we train at the native 32×32 resolution and normalize images to $[-1, 1]$; for visualization only, we upsample to 64×64 using nearest-neighbor interpolation. For **CelebA-64**, we center-crop faces, resize to 64×64 , and normalize to $[-1, 1]$. For **LSUN Bedroom/Church-64**, we apply a square center-crop, resize to 64×64 , and normalize to $[-1, 1]$.

F.3 Architectures

We adopt a residual DCGAN-style backbone because it offers a good balance between stability and capacity at the 64×64 resolution. The discriminator (critic) does not use BatchNorm in order to avoid interactions with gradient penalties. When spectral methods are used, we treat residual paths carefully.

Generator g_φ (latent $\dim z = 64$). A linear layer projects $z \sim \mathcal{N}(0, I_{64})$ to a $4 \times 4 \times (4 \cdot \text{GF})$ feature map. We then apply a stack of upsampling residual blocks whose depth depends on the target resolution: four blocks for 64×64 (CelebA and LSUN) and three blocks for 32×32 (CIFAR-10).

Discriminator (critic) \tilde{h}_θ . The critic receives images at dataset resolution and applies a stack of down-sampling residual blocks mirroring the generator. For 64×64 , we use four downsampling residual blocks with stride-2 3×3 convolutions (or the standard ResBlockD average-pool projection), two 3×3 convolutions per block, and LeakyReLU activations with negative slope 0.2; the skip path uses a stride-2 1×1 projection. For 32×32 , we use three downsampling residual blocks of the same design. A global sum-pool feeds a linear head that outputs the raw scalar $\tilde{h}_\theta(x)$. Unless otherwise noted, the critic uses no BatchNorm (i.e., we only consider instance or layer normalization in explicit ablations).

F.4 Objectives and Priors

We estimate the prior-weighted BOLT objective on mini-batches using the bounded score $h = \sigma(\tilde{h})$. The critic maximizes the BOLT gap, whereas the generator minimizes it. We set the real/fake prior to $\pi = 0.5$ by default. For $\{x_j\}_{j=1}^B \sim P_{\text{data}}$ and $\{\hat{x}_j\}_{j=1}^B \sim P_g$, let $f_j = \tilde{h}_\theta(x_j)$, $\hat{f}_j = \tilde{h}_\theta(\hat{x}_j)$, $h_j = \sigma(f_j)$, and $\hat{h}_j = \sigma(\hat{f}_j)$. The mini-batch estimator is then

$$\mathcal{L}_{\text{BOLT}}(\varphi, \theta) = \pi \frac{1}{B} \sum_{j=1}^B h_j - (1 - \pi) \frac{1}{B} \sum_{j=1}^B \hat{h}_j.$$

F.5 Lipschitz Enforcement

We enforce approximate 1-Lipschitz behavior of the critic using the WGAN-GP gradient penalty applied to the *raw* score \tilde{h}_θ . Concretely, we sample interpolants $\tilde{x} = \alpha x + (1 - \alpha)\hat{x}$ with $\alpha \sim \text{Unif}[0, 1]$ and add

$$\text{GP} = \frac{\lambda_{\text{GP}}}{B} \sum_{j=1}^B \left(\|\nabla_{\tilde{x}_j} \tilde{h}_\theta(\tilde{x}_j)\|_2 - 1 \right)^2$$

to the critic objective. We set $\lambda_{\text{GP}} = 10$ as our default because this value is the *de facto* choice introduced by WGAN-GP and widely adopted in subsequent implementations; it offers a robust trade-off between stability and capacity in practice (Gulrajani et al., 2017; Mescheder et al., 2018). In Appendix F we also report a small sweep over $\lambda_{\text{GP}} \in \{1, 5, 10, 20\}$ that confirms the default is near-optimal under our settings.

F.6 Optimization and Training Schedule

We optimize both networks with Adam using $\beta_1 = 0.5$, $\beta_2 = 0.999$, and learning rates $\eta_d = \eta_g = 2 \times 10^{-4}$. Each iteration performs $n_d = 5$ critic updates followed by one generator update, a ratio that we found to be consistently reliable across datasets. Unless otherwise stated, the learning rate is held constant. We optionally maintain an exponential moving average (EMA) of the generator parameters with decay 0.999 for evaluation, but we leave EMA off by default to match baseline comparisons. The batch size is $B = 64$; when memory is limited, we use gradient accumulation to preserve the effective batch size. Unless otherwise specified, figures correspond to the 20-epoch checkpoint.

F.7 Training Algorithm (Overview and Pseudocode)

Each iteration draws a batch of real samples and a batch of latent codes, produces fake samples, and computes both raw scores \tilde{h} and bounded scores $h = \sigma(\tilde{h})$. We then form the mini-batch BOLT objective, evaluate the gradient penalty along line-segment interpolants, and update the critic by maximizing the BOLT gap (equivalently, minimizing $-\mathcal{L}_{\text{BOLT}} + \text{GP}$). Next, we draw a fresh latent batch and update the generator to minimize the same BOLT gap by reducing the fake-score term. Algorithm 1 summarizes the procedure.

F.8 Hyperparameter Sweeps and Selection

We sweep $\lambda_{\text{GP}} \in \{1, 5, 10, 20\}$ separately for each method and dataset, and we report the best FID per method within a fixed compute budget. Other knobs such as β_1 and n_d have a comparatively minor effect in our ranges (e.g., within ± 1 FID on CIFAR-10).

F.9 Evaluation Metrics

Fréchet Inception Distance (FID). We use FID as the primary quantitative measure of image-generation quality. FID computes the Fréchet distance between multivariate Gaussian embeddings of real and generated images in the feature space of a pre-trained Inception-V3 network (Heusel et al., 2017). Lower values indicate that the generated distribution is closer to the real distribution in terms of both perceptual and statistical similarity. Unless noted otherwise, all FID scores are computed on 10k generated samples using the official Inception statistics for each dataset.

Evaluation Protocol. Unless stated otherwise, we evaluate every checkpoint with 10k samples and the official Inception statistics. Snapshot selection and the choice of λ_{GP} follow the settings detailed in Appendix F.

F.10 Logging and Diagnostics

We monitor diagnostics that directly reflect Lipschitz control and training health. In particular, we track the empirical distribution of $\|\nabla_{\tilde{x}} \tilde{h}_\theta(\tilde{x})\|_2$ on the interpolants used for the penalty, the value of the penalty

Algorithm 1 BOLT–GAN training with gradient penalty (notation matched to paper)

Require: • Discriminator (raw score) \tilde{h}_θ , generator g_φ
 • Data distribution P_{data} , latent distribution P_Z
 • Prior $\pi \in (0, 1]$
 • Batch size B , critic updates per generator update n_d
 • Learning rates η_d, η_g , iterations T
 • Gradient-penalty coefficient λ_{gp}
Ensure: trained parameters θ, φ

- 1: **for** iteration = 1 **to** T **do**
- 2: **for** $k = 1$ **to** n_d **do**
- 3: Sample $\{x_j\}_{j=1}^B \sim P_{\text{data}}$; sample $\{z_j\}_{j=1}^B \sim P_Z$; $\hat{x}_j \leftarrow g_\varphi(z_j)$
- 4: Raw scores: $f_j \leftarrow \tilde{h}_\theta(x_j)$, $\hat{f}_j \leftarrow \tilde{h}_\theta(\hat{x}_j)$; bounded: $h_j \leftarrow \sigma(f_j)$, $\hat{h}_j \leftarrow \sigma(\hat{f}_j)$
- 5: (a) *Batch estimator of $\mathcal{L}_{\text{BOLT}}$ for fixed θ :*

$$\mathcal{L}_{\text{BOLT}}(\varphi, \theta) = \pi \cdot \frac{1}{B} \sum_{j=1}^B h_j - (1 - \pi) \cdot \frac{1}{B} \sum_{j=1}^B \hat{h}_j$$

- 6: (b) *Gradient penalty on raw score (WGAN–GP style):*
- 7: Sample $\{\alpha_j\}_{j=1}^B \sim \text{Uniform}(0, 1)$; $\tilde{x}_j = \alpha_j x_j + (1 - \alpha_j) \hat{x}_j$

$$\text{GP} = \frac{\lambda_{\text{gp}}}{B} \sum_{j=1}^B \left(\|\nabla_{\tilde{x}_j} \tilde{h}_\theta(\tilde{x}_j)\|_2 - 1 \right)^2$$

- 8: (c) *Critic loss & update (maximize $\mathcal{L}_{\text{BOLT}}$):*

$$\mathcal{L}_\theta = -\mathcal{L}_{\text{BOLT}}(\varphi, \theta) + \text{GP} ; \quad \theta \leftarrow \theta - \eta_d \nabla_\theta \mathcal{L}_\theta$$

- 9: **end for**
- 10: *Generator update (minimize $\mathcal{L}_{\text{BOLT}}$):*
- 11: Sample $\{z'_j\}_{j=1}^B \sim P_Z$; $\hat{x}'_j \leftarrow g_\varphi(z'_j)$; $\hat{h}'_j \leftarrow \sigma(\tilde{h}_\theta(\hat{x}'_j))$

$$\mathcal{L}_\varphi = -(1 - \pi) \cdot \frac{1}{B} \sum_{j=1}^B \hat{h}'_j ; \quad \varphi \leftarrow \varphi - \eta_g \nabla_\varphi \mathcal{L}_\varphi$$

- 12: **end for**

term itself, and the ratio $\mathbb{E}[(\|\nabla\| - 1)^2]/\mathbb{E}[\text{critic term}]$. Healthy runs concentrate gradient norms near 1; persistent mass well above 1 suggests increasing λ_{GP} or applying the penalty more frequently, whereas mass well below 1 suggests reducing λ_{GP} or switching to a one-sided penalty.

F.11 Determinism and Seeds

For exact reproducibility we fix a global seed, propagate per-worker dataloader seeds, and set `torch.backends.cudnn.deterministic=True` and `benchmark=False`. We seed Python, NumPy, and PyTorch random number generators. We release configuration files, grid-reconstruction scripts, and commit hashes that match the figures and tables.

F.12 Failure Modes and Stability Notes

The non-Lipschitz BOLT variant ($\lambda_{\text{GP}} = 0$) frequently diverges or produces very high FID, which is consistent with optimizing a TV-strength objective. Combining strong spectral normalization with a large

gradient-penalty coefficient can over-regularize the critic; in such cases we prefer to rely primarily on a single Lipschitz control. We also avoid BatchNorm in the critic. If the critic saturates, reducing the discriminator learning rate or increasing n_d usually restores stable training. The training code is available in our anonymous repository.